J. Fluid Mech. (1994), *vol.* 274, *pp.* 43–68

Dynamics of vortical structures in a homogeneous shear flow

By SHIGEO KIDA[1] AND MITSURU TANAKA[2]

[1] Research Institute for Mathematical Sciences, Kyoto University, Kyoto 606-01, Japan

[2] Department of Physics, Faculty of Science, Kyoto University, Kyoto 606-01, Japan

(Received 13 August 1993 and in revised form 15 February 1994)

The mechanism of generation, development and interaction of vortical structures, extracted as concentrated-vorticity regions, in homogeneous shear turbulence is investigated by the use of the results of a direct numerical simulation of the Navier–Stokes equation with 128^3 grid points. Among others, a few of typical vortical structures are identified as important dynamical elements, namely longitudinal and lateral vortex tubes and vortex layers. They interact strongly with each other. Longitudinal vortex tubes are generated from a random fluctuating vorticity field through stretching of fluid elements caused by the mean linear shear. They are inclined toward the streamwise direction by rotational motion due to the mean shear. There is a small (about 10°) deviation in direction between the longitudinal vortex tubes and vorticity vectors therein, which makes the vorticity vectors turn toward the spanwise direction (against the mean vorticity) until the spanwise components of the fluctuating vorticity become comparable in magnitude with the mean vorticity. These longitudinal vortex tubes induce straining flows perpendicular to themselves which generate vortex layers with spanwise vorticity in planes spanned by the tubes and the spanwise axis. These vortex layers are unstable, and roll up into lateral vortex tubes with concentrated spanwise vorticity through the Kelvin–Helmholtz instability. All of these vortical structures, through strong mutual interactions, break down into a complicated small-scale random vorticity field. Throughout the simulated period an oblique stripe structure dominates the whole flow field: initially it is inclined at about 45° to the downstream and, as the flow develops, the inclination angle decreases but eventually stays at around 10°–20°.

1. Introduction

Coherent structures, such as tubes and layers of concentrated vorticity, are observed to prevail for relatively long times in fully developed turbulence. They are expected to play a central role in turbulence dynamics. The transport processes of heat, mass, momentum and kinetic energy in turbulent flows seem to be controlled by coherent structures. The bursting process in turbulent boundary layers is considered to be triggered by hairpin vortices. Understanding their structure and dynamics is indispensable for modelling and controlling turbulence.

In homogeneous isotropic turbulence, tube-like structures of concentrated-vorticity regions have been observed numerically by many researchers (Siggia 1981; Kerr 1985; Hosokawa & Yamamoto 1989; She, Jackson & Orszag 1990; Vincent & Meneguzzi 1991). In homogeneous shear turbulence, which we deal with in this paper, Rogers & Moin (1987) demonstrated the existence of hairpin vortices. Other coherent structures

include the rib structure in free shear turbulence (Jiménez, Cogollos & Bernal 1985; Hussain 1986) and streamwise streaks (Kline *et al.* 1967; Kim & Moin 1986).

Numerically, concentrated-vorticity regions are visualized by iso-surfaces of high vorticity magnitude. It is not easy to discriminate vortex tubes and layers only in terms of vorticity magnitude. Recently, a visual recognition diagnostic technique to extract vortex tubes and layers was developed by the present authors (Tanaka & Kida 1993). Vortex tubes are characterized as regions of large vorticity and small shear, whereas vortex layers are regions of large vorticity and comparative large shear. Note here that whenever vorticity dynamics is discussed, attention should be paid to the difference in definition between iso-surfaces of vorticity magnitude and vorticity surfaces (Kida & Takaoka 1994). Also, note that iso-surfaces of vorticity do not always imply a sharp discontinuity in vorticity distribution even though it may appear so for a continuously distributed vorticity field (§4.1).

We study here the dynamics of vortical structures in homogeneous shear turbulence which is realized by solving the Navier–Stokes equation numerically (Kida & Tanaka 1992). Some of the global behaviour, the statistics and the nature of coherent vortex tubes of this flow field have already been reported in Kida & Tanaka (1992). It was observed that the amplitude of the fluctuating velocity increases exponentially in time, but the development of the flow field seems to be statistically similar (cf. Tavoularis 1985; Tavoularis & Karnik 1989). Many complicated vortical structures develop and interact with each other in a randomly fluctuating background vorticity field. Typical vortical structures include longitudinal vortex tubes directed nearly in the streamwise direction, lateral vortex tubes along the spanwise direction, and vortex layers with spanwise vorticity. The main purpose of this paper is to explore the mechanism of generation, development, interaction and breakdown of these vortical structures. The configuration of the homogeneous shear flow and the numerical method are briefly described in §2. Results of the numerical simulation and an analytical consideration of the dynamical development of various vortical structures are presented in §§3 and 4. Section 5 is devoted to further discussion of the dynamics of vortical structures.

2. Formulation

2.1. *Homogeneous shear flow*

We consider the motion of an incompressible viscous fluid in a linear mean shear $(Sx_2, 0, 0)$ which is along the x_1-direction and varies linearly with x_2 (figure 1). The mean vorticity is therefore uniform in space and is directed towards the negative x_3-axis. Here, the x_1-, x_2- and x_3-axes will be called, for brevity, *streamwise*, *vertical*, and *spanwise* directions, respectively. The fluctuating velocity field can be homogeneous in such a linear mean shear flow.

The time-evolution of the fluctuating velocity field $\boldsymbol{u} = (u_1, u_2, u_3)$ is described by the Navier–Stokes equation

$$\frac{\partial u_i}{\partial t} = -Sx_2\frac{\partial u_i}{\partial x_1} - Su_2\delta_{i1} - u_j\frac{\partial u_i}{\partial x_j} - \frac{\partial p}{\partial x_i} + \nu\nabla^2 u_i \quad (i = 1, 2, 3), \tag{2.1}$$

supplemented by the continuity equation

$$\frac{\partial u_j}{\partial x_j} = 0, \tag{2.2}$$

where p is the pressure and ν is the kinematic viscosity. The fluid density is assumed to be uniform and be unity. A summation is taken over 1–3 for repeated subscripts.

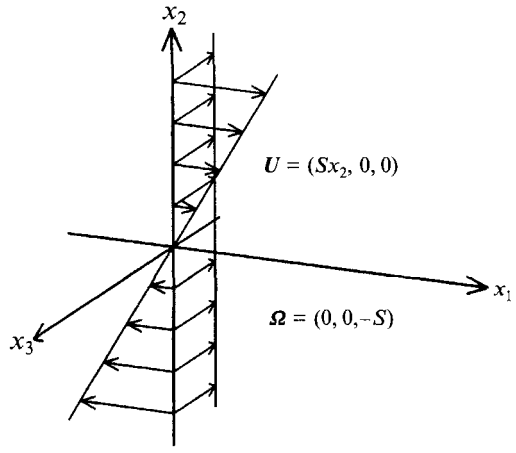

FIGURE 1. Configuration of homogeneously sheared flow. The x_1-, x_2- and x_3-axes are called the streamwise, vertical and spanwise directions, respectively.

By taking the curl of (2.1), we obtain the vorticity equation

$$\frac{\partial \omega_i}{\partial t} = \left(-Sx_2\frac{\partial \omega_i}{\partial x_1} - u_k\frac{\partial \omega_i}{\partial x_k}\right) + \left(S\omega_2\delta_{i1} - S\frac{\partial u_i}{\partial x_3} + \omega_k\frac{\partial u_i}{\partial x_k}\right) + \nu\nabla^2\omega_i \quad (i = 1, 2, 3), \tag{2.3}$$

where

$$\omega_i = \epsilon_{ijk}\frac{\partial u_k}{\partial x_j} \quad (i = 1, 2, 3) \tag{2.4}$$

is the fluctuating vorticity, and ϵ_{ijk} is the Eddington alternating tensor.

The first term in the first brackets on the right-hand side of (2.3) represents the advection of vorticity by the mean shear which makes the spatial structure of vorticity incline toward the streamwise direction without changing the direction of vorticity vector. The second term describes the advection of vorticity by the fluctuating velocity. The three terms in the second brackets contribute to the tilting and stretching of vorticity lines, or to the change of direction and intensity of the vorticity vector. The first one describes a conversion of vorticity from the vertical to the streamwise components by the mean shear. The second represents either a conversion of vorticity from the mean vorticity to the x_i-component ($i \neq 3$) or a change in intensity of the spanwise vorticity ($i = 3$). Likewise, the third one describes either a conversion of vorticity from the x_k-component to the x_i-component ($k \neq i$) or a change in intensity of vorticity by stretching or contraction of vorticity lines ($k = i$). Finally, the last term represents viscous diffusion.

There are three non-dimensional parameters that characterize this problem. The shear rate parameter

$$S^*(t) = \frac{u'^2/\epsilon}{1/S} = \frac{Su'^2}{\nu\omega'^2} \tag{2.5}$$

represents the ratio of the characteristic time of the nonlinear interaction of fluctuating velocity to that of the mean shear (Lee, Kim & Moin 1990). Here, u' is the r.m.s. of the fluctuating velocity, ω' is that of the vorticity, and ϵ is the mean energy dissipation rate. The Reynolds number

$$R_\lambda(t) = \frac{u'^2/\epsilon}{1/\omega'} = \frac{u'^2}{\nu\omega'} \tag{2.6}$$

represents the ratio of the characteristic time of the nonlinear interaction to that of the viscous effects. The third parameter which characterizes the simulation is $R_L = L/(u'^3/\epsilon)$, the ratio between the numerical box size L ($= 2\pi$, see §2.2) and the turbulence lengthscale u'^3/ϵ. This measures the effect of box size on the numerical flow: the larger the value of R_L, the smaller the effect. In the simulation discussed in the following, R_L is initially 3.1, then increases to a maximum of 4.1 at $St = 1.84$, and then decreases to 1.3 at $St = 14$. Hence, the effect of box size is considered not to be significant.

2.2. *Numerical method*

We solve (2.1) and (2.2) numerically under periodic boundary conditions. In order to eliminate the explicit appearance of the space coordinate x_2 in (2.1) we introduce a coordinate system $\boldsymbol{x}'$ that is advected by the mean shear flow as $x_1' = x_1 - Stx_2$, $x_2' = x_2$, $x_3' = x_3$ (Rogallo 1981). The flow field is periodic in this moving coordinate system. The numerical simulation is performed in the domain $0 \leqslant \frac{1}{2}x_1', x_2', x_3' \leqslant 2\pi$. Note that the period in the streamwise direction is the double those in the other two directions.

The velocity field is expanded into a Fourier series as

$$\boldsymbol{u}(\boldsymbol{x}', t) = \sum_{\boldsymbol{k}'} \tilde{\boldsymbol{u}}(\boldsymbol{k}', t) \exp[\mathrm{i}\boldsymbol{k}' \cdot \boldsymbol{x}'], \tag{2.7}$$

where $\boldsymbol{k}' = (k_1', k_2', k_3')$ is the wavenumber, $2k_1', k_2', k_3'$ being integers. The summation is taken over $-\frac{1}{2}N < 2k_1', k_2', k_3' \leqslant \frac{1}{2}N$, where $N = 128$. The Fourier coefficient $\tilde{\boldsymbol{u}}(\boldsymbol{k}', t)$ is a complex variable with the property that $\tilde{\boldsymbol{u}}(-\boldsymbol{k}', t) = \tilde{\boldsymbol{u}}^*(\boldsymbol{k}', t)$, where $*$ denotes the complex conjugate.

Because the moving frame is distorted more and more as time progresses, we remesh it every 2 time units, i.e. at $St = 1, 3, 5, \ldots$, at which the moving frame is skewed just by half (Rogallo 1981). The remeshing is done by using the periodic boundary condition in the streamwise direction. After a remeshing, the grid is skewed by the same amount in the opposite sense. This new grid continues to be distorted in time and another remeshing is necessary. The moving grid happens to be orthogonal at $St = 0, 2, 4, \ldots$. The Fourier modes ($|k_2| \geqslant \frac{1}{2}N - |k_1|$) which may cause aliasing errors at remeshing are set to be zero at every time step. This avoids a sudden decrease of energy and enstrophy at remeshing. Actually the loss of enstrophy per unit time was a few percent of the total. The present numerical scheme is the same as Rogallo's (1981) except for this last point.

The spectral method is used for calculation of the nonlinear terms in the Navier–Stokes equation. The grid spacings are $\Delta x_1 = 2\Delta x_2 = 2\Delta x_3 = 4\pi/N$ ($\approx 3.1 l_s$, see below), where

$$l_s = (\nu/S)^{1/2} \tag{2.8}$$

is a lengthscale at which the mean strain and viscous effects balance. The Runge–Kutta–Gill scheme (fourth-order accuracy) is employed for the time integration.

By expecting that the turbulence dynamics in the developed stage may be insensitive to the initial velocity field, we employ here a simple one which is composed of relatively large-scale motions. The initial velocity field is given with Fourier coefficients $\tilde{\boldsymbol{u}}(\boldsymbol{k}, 0)$ with random phase and with a prescribed energy spectrum of the form

$$E(k) = ck^4 \exp[-2k^2/k_0^2], \tag{2.9}$$

c and k_0 being constants. This spectrum has a peak at a wavenumber k_0, i.e. at a lengthscale $\frac{1}{2}k_0 \Delta x_1 = k_0 \Delta x_2 = k_0 \Delta x_3$. Many realizations are simulated with different values

of $S^*(0)$ and $R_\lambda(0)$ with the initial energy spectrum (2.9). The time evolution of the fluctuating velocity field behaves quite differently depending on the values of $S^*(0)$ and $R_\lambda(0)$ (Kida & Tanaka 1993, and work in preparation; see also Rogers & Moin 1987; Lee *et al.* 1990). For $S^*(0)$ larger than some critical value S_c^* (≈ 10) the enstrophy increases monotonically in time. For smaller values of $S^*(0) < S_c^*$, on the other hand, the enstrophy decreases during a substantial period of the simulation though it shows some tendency to increase at later times. As the flow develops, $R_\lambda(t)$ seems to increase without limit, whereas $S^*(t)$ approaches some value around 10 which is close to S_c^*.

Here, we concentrate our attention on a single realization in which the three important terms, i.e. the mean strain, the nonlinear self-interaction and the viscous terms, may play comparable roles. We take $c = 1.93 \times 10^{-4}$ and $k_0 = \sqrt{50}$ (≈ 7) so that the initial velocity and vorticity fluctuations are $u'^2 = 1.6$ and $\omega'^2 = 100$, respectively. The shear rate S is set to be 10, the viscosity ν is 0.01 (therefore $S^*(0) = 16$, $R_\lambda(0) = 16$ and $l_s \approx 0.03$). The ratio of the r.m.s. of vorticity and the shear rate is 1 at the initial instant. The intensity of the initial random vorticity is comparable in magnitude with the mean shear. To examine the role of the nonlinear interaction in the fluctuating velocity field a rapid-distortion calculation, in which the nonlinear terms in the fluctuations in (2.3) are discarded, was also performed with the same initial condition. We integrated 800 steps with time-increment 0.002 so that the final time simulated is 1.6 ($0 \leqslant St \leqslant 16$). It took 24 s per time step on the FACOM VP2600 at Kyoto University.

3. Characteristics of the flow field

3.1. *High-vorticity region*

The time-evolution of the anisotropy tensor of vorticity

$$v_{ij} = \frac{\langle \omega_i \omega_j \rangle}{\langle \omega_k \omega_k \rangle} - \tfrac{1}{3}\delta_{ij}, \tag{3.1}$$

where $\langle\ \rangle$ denotes the spatial average, describes a global feature of the development of the vorticity field (figure 2). Because the present flow configuration is symmetric with respect to the x_3-axis, i.e. invariant under a coordinate transformation $(x_1, x_2) \to (-x_1, -x_2)$, two non-diagonal elements, v_{13} and v_{23} should be zero within statistical fluctuations. The anisotropy tensor is zero at the initial instant because the initial fluctuating vorticity field is isotropic. The relative magnitude of the three diagonal elements, $v_{11} > v_{22} > v_{33}$, during the initial stage ($St \lesssim 2$) seems to be universal for any isotropic initial flow field. This ordering is caused by stretching and rotating motions of the mean shear (§4.1).

The non-diagonal element v_{12} increases much faster than the diagonal elements at the early stage of evolution. The positiveness of v_{12} implies that the fluctuating vorticity is inclined toward the streamwise direction in such a way that $\omega_1 \omega_2 > 0$, which is a direct consequence of the fact that the direction of maximal expansion of the linear mean shear is inclined at 45° to the downstream. All of this early-time behaviour of the anisotropic tensor is predicted by rapid distortion theory (see figure 3 of Kida & Tanaka 1992; Lee *et al.* 1990).†

† The initial increase of the anisotropy tensor from an isotropic state is explicitly calculated in the rapid distortion approximation (Townsend 1970) in which nonlinear self-interaction and viscous terms are neglected in (2.3). The result is $v_{11} \approx \frac{1}{5}t^2$, $v_{22} \approx \frac{2}{15}t^2$, $v_{33} = O(t^3)$, $v_{12} \approx \frac{1}{3}t$ for small time t. Note that the initial increase of v_{12} is proportional to t, which is much faster than the other components.

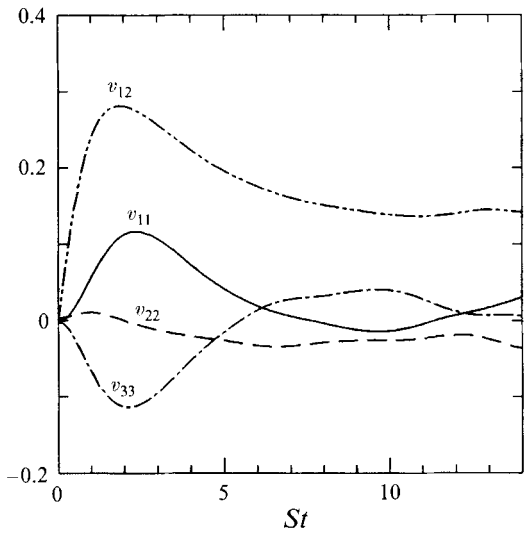

FIGURE 2. Time-evolution of the anisotropy tensor of the vorticity $v_{ij} = \langle \omega_i \omega_j \rangle / \langle \omega_k \omega_k \rangle - \frac{1}{3}\delta_{ij}$.

The most prominent feature in the development of the anisotropy tensor at the later stage ($2 \lesssim St \lesssim 10$) is a rapid increase of the spanwise element v_{33}. As will be discussed in §4.2, the spanwise component of fluctuating vorticity ω_3 is generated from the mean shear through a spanwise vortex stretching, and therefore has the same sign as the mean vorticity. The rapid increase of spanwise element v_{33} leads to a relative decrease of streamwise element v_{11}, while the vertical element v_{22} does not change very much. The non-diagonal element v_{12} reaches a maximum at $St \approx 2$, and then decreases gradually to about 0.15. The flow field tends to be isotropic at around $St = 12$, but later it deviates from isotropy again. Current work by the authors with many realizations with different values of $S^*(0)$ and $R_\lambda(0)$ suggests that there may be a common tendency in the relative magnitude of elements of the anisotropy tensor at later times. The above behaviour of the anisotropy tensor can be explained by the generation and development of various vortical structures (§4).

The spatial structure of the vorticity field is most conveniently visualized from the iso-surface of vorticity magnitude. In figure 3, we plot the iso-surface in one half of the computed domain ($0 \leqslant x_1, x_2, x_3 \leqslant 2\pi$) at times $St = 0$, 0.4, 2, 6, 10 and 14. The mean flow direction is horizontal and changes linearly in the vertical direction. The magnitude of the vorticity on the surfaces is different at different times, but is between twice and three times the r.m.s. values. The vorticity field is isotropic at the initial instant. At an early time ($St = 0.4$) high-vorticity blobs are being stretched in a direction inclined at 45° to the downstream. Elongated high-vorticity regions are discernible at $St = 2$. These long thin high-vorticity regions are called *longitudinal vortex tubes*. At later times (e.g. at $St = 6$) the longitudinal vortex tubes incline more toward the streamwise direction, and at the same time there emerge many layer-like structures (see figure 4 below). Some of the layers have already appeared by $St = 2$.

FIGURE 3. Iso-surfaces of vorticity magnitude. (*a*) $St = 0$, $0 \leqslant x_1/\Delta x_1 \leqslant 63$, $|\omega| = 2S = 2\omega'$; (*b*) $St = 0.4$, $0 \leqslant x_1/\Delta x_1 \leqslant 63$, $|\omega| = 2.1S = 2.1\omega'$; (*c*) $St = 2$, $0 \leqslant x_1/\Delta x_1 \leqslant 63$, $|\omega| = 2.9S = 2.3\omega'$; (*d*) $St = 6$, $0 \leqslant x_1/\Delta x_1 \leqslant 63$, $|\omega| = 3.84S = 2.3\omega'$; (*e*) $St = 10$, $0 \leqslant x_1/\Delta x_1 \leqslant 63$, $|\omega| = 5.56S = 2.6\omega'$; (*f*) $St = 14$, $64 \leqslant x_1/\Delta x_1 \leqslant 127$, $|\omega| = 8.6S = 2.9\omega'$. $0 \leqslant x_2/\Delta x_2$, $x_3/\Delta x_3 \leqslant 127$.

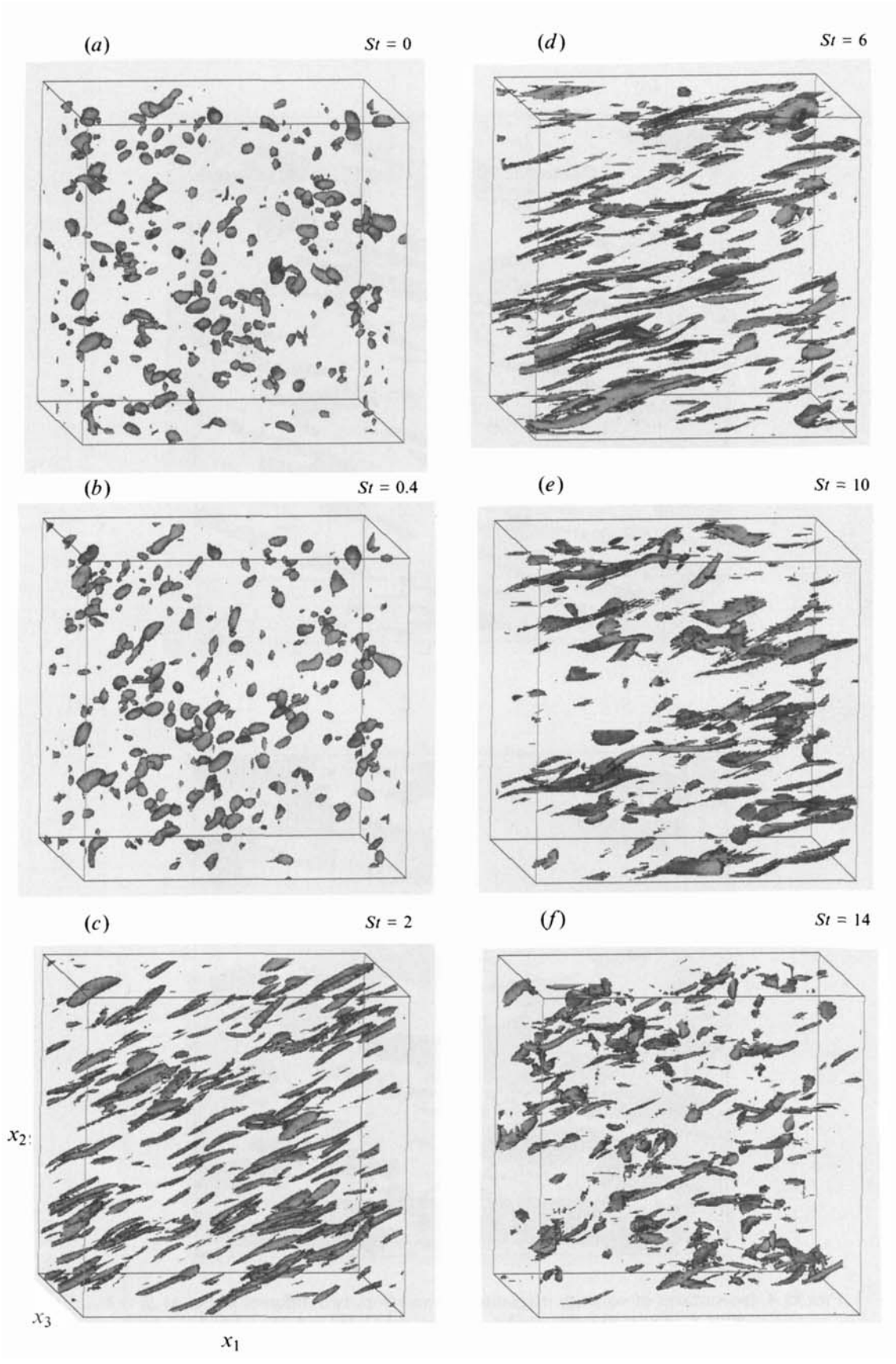

FIGURE 3. For caption see facing page.

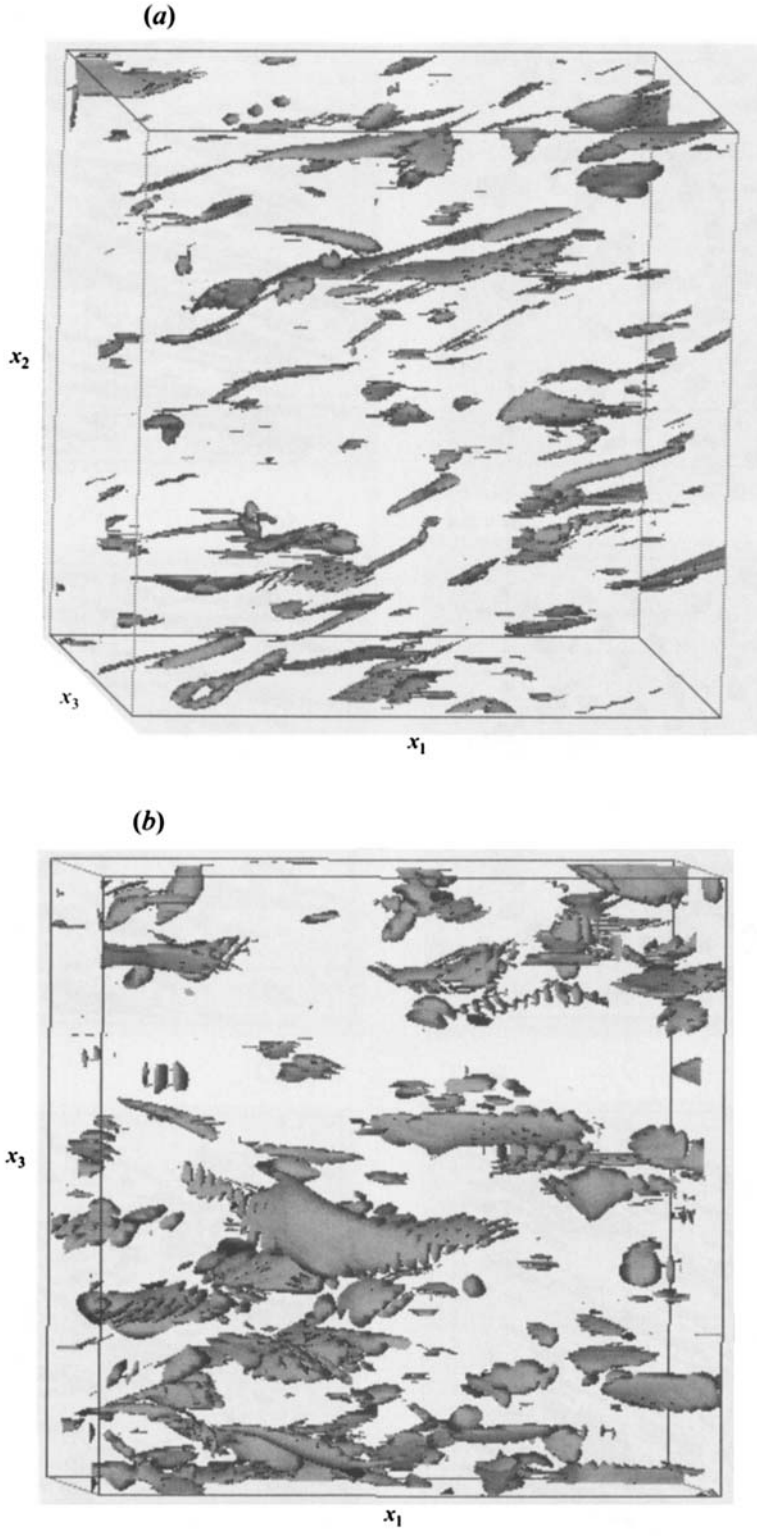

FIGURE 4. Iso-surfaces of vorticity magnitude viewed from two different angles at $St = 8$. $50 \leqslant x_1/\Delta x_1 \leqslant 113$, $0 \leqslant x_2/\Delta x_2$, $x_3/\Delta x_3 \leqslant 127$, $|\omega| = 4.7S = 2.5\omega'$.

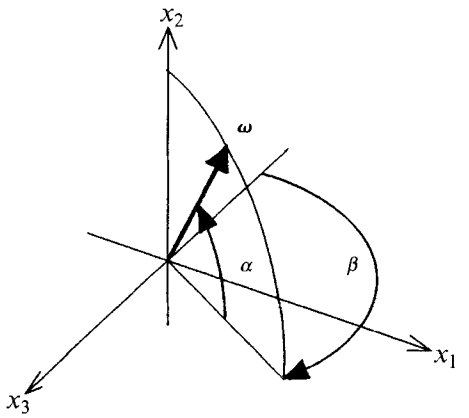

FIGURE 5. Definition of orientation angles α and β of vorticity vector ω.

The vortical structures, both the vortex tubes and layers, break down at later stages ($St \gtrsim 12$) at which smaller structures appear and the flow field becomes more isotropic.

Vortex layers are more clearly seen in a plan view on the horizontal (x_1, x_3)-plane. We draw in figure 4(a, b) the iso-vorticity surfaces at $St = 8$ viewed from two different angles. Layer-like structures which extend over several tens of mesh sizes in the streamwise direction and nearly ten mesh sizes in the spanwise one are clearly observed. These layers are wavy but nearly parallel to the spanwise direction.

3.2. *Vorticity directions*

In order to examine the distribution of the direction of the vorticity vectors quantitatively we introduce two orientation angles α and β, which are called the vertical and horizontal angles respectively, of the direction of a vorticity vector (figure 5). We have the following relations:

$$\omega_1 = |\boldsymbol{\omega}| \cos\alpha \sin\beta, \quad \omega_2 = |\boldsymbol{\omega}| \sin\alpha, \quad \omega_3 = -|\boldsymbol{\omega}| \cos\alpha \cos\beta. \tag{3.2}$$

Remember that the origin $(\alpha, \beta) = (0°, 0°)$ corresponds to the negative x_3-axis, i.e. the direction of vorticity of the mean shear.

In figure 6(a), we show the probability density function (PDF) $P(\alpha, \beta)$ of the orientation angles of fluctuating vorticity weighted by $|\boldsymbol{\omega}|$ at times $St = 0.4$, 2, 6, 10 and 14. Here, $P(\alpha, \beta) \cos\alpha \Delta\alpha \Delta\beta$ is proportional to $|\boldsymbol{\omega}|$ times the number of grid points on which the orientation angles of $\boldsymbol{\omega}$ lie in domain $(\alpha - \frac{1}{2}\Delta\alpha, \alpha + \frac{1}{2}\Delta\alpha)$ and $(\beta - \frac{1}{2}\Delta\beta, \beta + \frac{1}{2}\Delta\beta)$, where $\Delta\alpha = \Delta\beta = 5°$. The distribution is symmetric with respect to the origin, which reflects the invariance of the flow configuration by a rotation of angle 180° around the x_3-axis. At an earlier time ($St = 0.4$), two peaks appear at $(\alpha_{peak}, \beta_{peak}) = \pm(45°, 90°)$ which are the directions of maximal expansion of the mean shear $(Sx_2, 0, 0)$ (Rogers & Moin 1987). As time goes on, the peaks become sharper, representing longitudinal vortices that are being generated. They move toward $(\alpha, \beta) = (0°, \pm 180°)$, respectively (shown by arrows in the top panel); namely, the fluctuating vorticity tends to incline toward streamwise direction while turning to the opposite direction to that of vorticity of the mean shear. A mechanism of the change in direction of the vorticity vectors will be discussed in §4.1. This movement, however, decelerates at later times and the positions of the peaks eventually stay around $(\alpha_{peak}, \beta_{peak}) = \pm(20°, 130°)$. These statistically equilibrium angles are probably maintained by some complicated balance in the mutual interactions among various vortical structures.

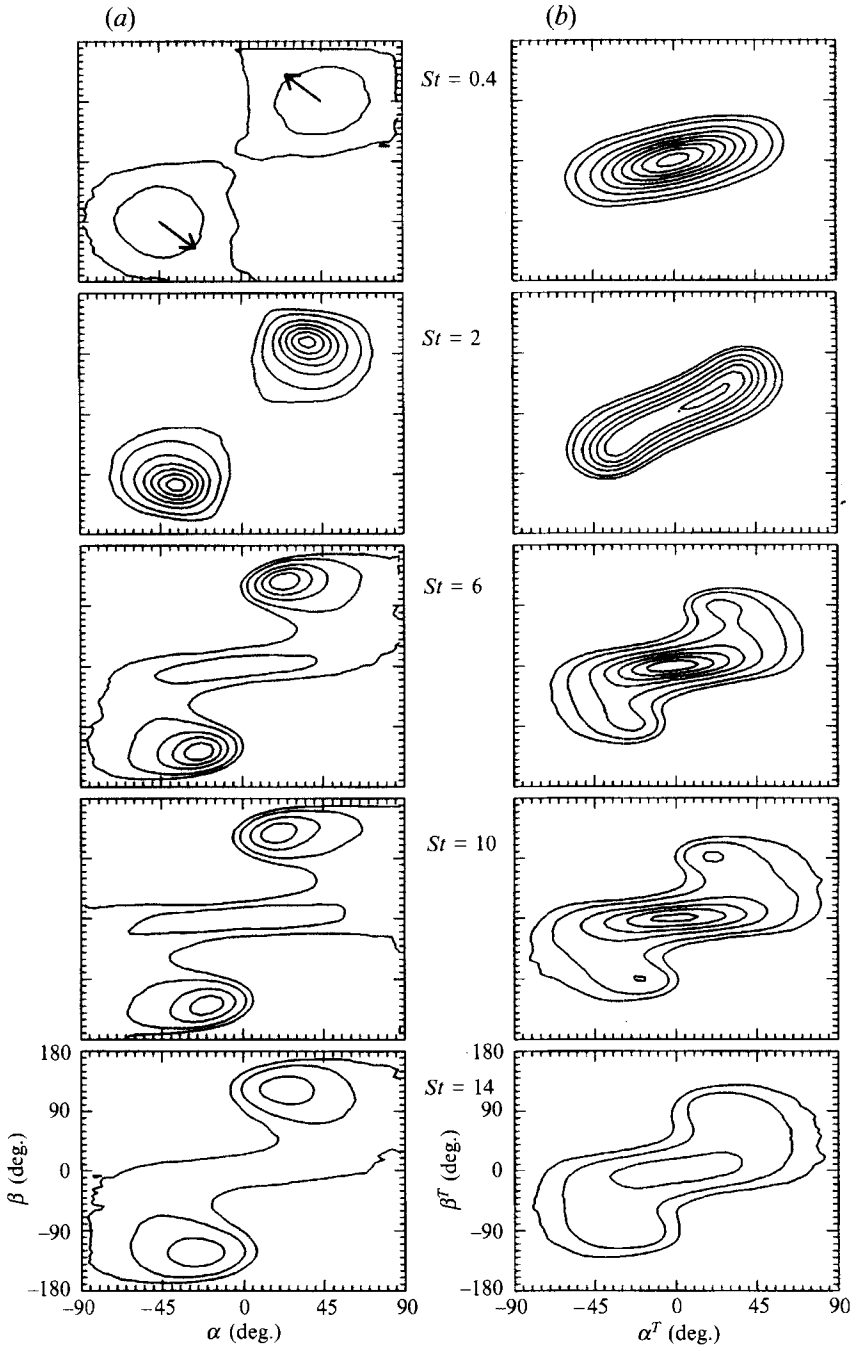

FIGURE 6. Probability density functions of orientation angles α and β of (*a*) the fluctuating vorticity and (*b*) the total vorticity, weighed by $|\omega|$ and $|\omega^T|$, respectively. Contour levels are 1.0, 1.5, 2.5, 3.5, ... Arrows in the top panel denote the direction of movement of the peaks.

One more interesting feature in this figure is that another peak appears around the origin after $St = 6$, which disappears at $St = 14$. Vorticity vectors corresponding to this peak point in the direction of the mean-shear vorticity. As will be discussed in §4.2, this peak corresponds to vortex layers generated in around this period.

We also examine the total vorticity, which is the sum of the mean shear vorticity and fluctuating vorticity,

$$\boldsymbol{\omega}^T = \boldsymbol{\omega} - S\hat{\boldsymbol{x}}_3, \tag{3.3}$$

where $\hat{\boldsymbol{x}}_3$ is a unit vector in the spanwise direction. The PDF weighted by $|\boldsymbol{\omega}^T|$ of the orientation angle (α^T, β^T) of the total vorticity vector is shown in figure 6(*b*) (cf. Rogers & Moin 1987). At an early time ($St = 0.4$) longitudinal vortices have not fully developed yet and the mean vorticity in the negative x_3-direction is dominant, which manifests itself as a single peak at the origin. At $St = 2$, a straight ridge develops along a line $\alpha^T = \beta^T$, which is not very steep.

There are two prominent features in the PDF at later times ($St > 6$). One is round peaks at $(\alpha^T_{peak}, \beta^T_{peak}) = \pm(30°, 90°)$. These peaks correspond to longitudinal vortex tubes. It is interesting that the horizontal peak angle β^T_{peak} is $\pm 90°$, i.e. longitudinal vortex tubes, defined in terms of *total* vorticity, are aligned perpendicularly to the mean vorticity. No clear-cut explanation exists, however. In Rogers & Moin (1987) these peaks are discussed with relation to the orientation angles of legs of hairpin vortices. The other feature is a peak around the origin. This peak is thin in horizontal angle β and wide in vertical angle α. This corresponds to wavy vortex layers, the vorticity in which is perpendicular to longitudinal vortex tubes (§4.2).

Non-weighted (i.e. not multiplied by $|\boldsymbol{\omega}|$) PDFs of angles α and β for fluctuating and total vorticity exhibit a similar behaviour to the weighted ones with minor differences (figures omitted). The vertical angle α of the peaks of the weighted PDF is closer to 0° than that of the unweighted PDF by about 5°, at least for $t < 12$, implying that stronger vorticity is more inclined to the streamwise direction. The peak around the origin is more emphasized in the weighted PDF than in the unweighted one. In particular, the peak level is lower for the fluctuating vorticity in the unweighted PDF. This implies that vortex layers are composed of a large spanwise component of vorticity.

The movement of individual orientation angles α and β may give helpful information for understanding the dynamics of vortical structures. By taking time derivatives of (3.2), we obtain

$$\frac{\mathrm{D}\alpha}{\mathrm{D}t} = \frac{1}{|\boldsymbol{\omega}|}\left(-\sin\alpha\sin\beta\frac{\mathrm{D}\omega_1}{\mathrm{D}t} + \cos\alpha\frac{\mathrm{D}\omega_2}{\mathrm{D}t} + \sin\alpha\cos\beta\frac{\mathrm{D}\omega_3}{\mathrm{D}t}\right), \tag{3.4a}$$

$$\frac{\mathrm{D}\beta}{\mathrm{D}t} = \frac{1}{|\boldsymbol{\omega}|\cos\alpha}\left(\cos\beta\frac{\mathrm{D}\omega_1}{\mathrm{D}t} + \sin\beta\frac{\mathrm{D}\omega_3}{\mathrm{D}t}\right), \tag{3.4b}$$

where $\mathrm{D}/\mathrm{D}t$ denotes the Lagrangian derivative. Since $\mathrm{D}\boldsymbol{\omega}/\mathrm{D}t$ is known from (2.3), the mean values of $\mathrm{D}\alpha/\mathrm{D}t$ and $\mathrm{D}\beta/\mathrm{D}t$ weighted by $|\boldsymbol{\omega}|$ can be calculated at every (α, β) in the same way as $P(\alpha, \beta)$.

The time-derivative field $(\mathrm{D}\alpha/\mathrm{D}t, \mathrm{D}\beta/\mathrm{D}t)$ of the orientation angles at $St = 0.4$ thus obtained is shown by arrows in figure 7(*a*). The contour line of $P(\alpha, \beta)$ is drawn for reference (cf. figure 6*a*). There are two sources, at $(\alpha, \beta) = \pm(45°, -90°)$, and two sinks, at $(\alpha, \beta) = \pm(45°, 90°)$. The former is the direction of maximal contraction of the linear mean shear, while the latter is the direction of maximal expansion. Every orientation angle moves toward the direction of the maximal expansion. This is the mechanism of the generation of longitudinal vortex tubes (§4.1).

The time-derivative field $(\mathrm{D}\alpha^T/\mathrm{D}t, \mathrm{D}\beta^T/\mathrm{D}t)$ of the orientation angles for the total vorticity is calculated similarly. The result at $St = 6$ is shown in figure 7(*b*) together with a contour line of the PDF of (α^T, β^T) (cf. the third panel of figure 6*b*). This vector field exhibits a peculiar flow pattern. Starting from the origin, it moves to the

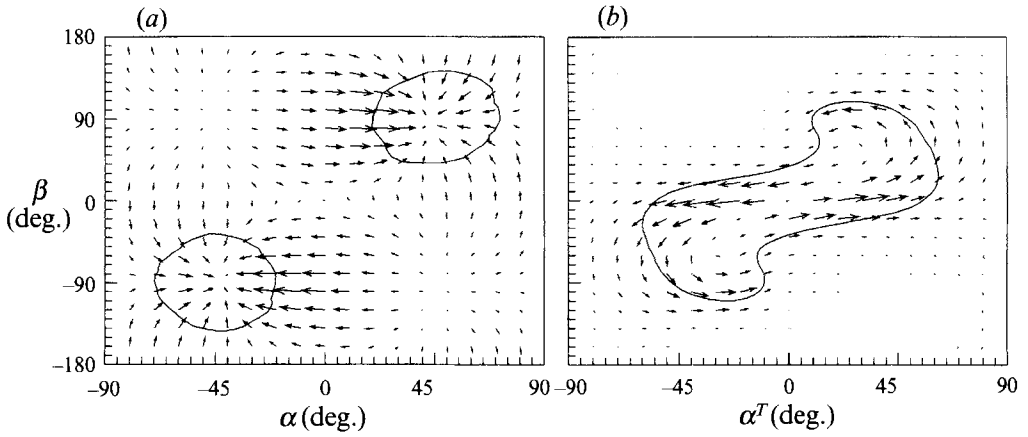

FIGURE 7. Movement of orientation angles. The time-derivative field ($D\alpha/Dt$, $D\beta/Dt$) of the orientation angles is shown by arrows (*a*) for the fluctuating vorticity at $St = 0.4$, and (*b*) for the total vorticity at $St = 6$. The contour line of the PDF of (α, β) at level of 1.5 is shown for reference.

right and left along a line $\beta^T = 0$ up to $|\alpha^T| = 40° \sim 60°$. Then the flow changes its direction toward larger $|\beta^T|$ until $|\beta^T| \approx 90°$. Remember here that the PDF of the orientation angles has peaks at $(\alpha^T_{peak}, \beta^T_{peak}) = \pm(30°, 90°)$ which roughly represents the mean orientation of longitudinal vortex tubes. Around these peaks the flow of the orientation angle again changes its direction in such a way that $|\alpha^T|$ decreases with little change of $|\beta^T|$. This flow pattern is commonly observed at other times ($St > 2$). Movement of this individual orientation angle from the origin to the peaks may represent 'undulation' of vortex layers in the spanwise direction and subsequent 'wrapping' or 'entrainment' into longitudinal vortex tubes (§4.2). The monotonical decrease of $|\alpha^T|$ after passing the peaks, on the other hand, indicates the perpetual leaning of longitudinal vortex tubes toward the streamwise direction (§4.1).

3.3. *Oblique structure*

The primary effect of the linear mean shear $(Sx_2, 0, 0)$ is to incline the flow structure toward the streamwise direction although there are complications because of three-dimensional interactions among vortical structures.

A global feature of the flow structure may be seen in the spatial correlation of vorticity. In figure 8(*a*, *b*), we draw the two-point correlation functions of the transverse component $(\omega_1^2+\omega_2^2)^{1/2} - \langle(\omega_1^2+\omega_2^2)^{1/2}\rangle$ and the spanwise component ω_3 in the transverse (x_1, x_2)-plane at $St = 0.4$, 2, 6, 10 and 14. They take a maximum at the origin which is normalized to be unity. The contour levels are 0.8, 0.4, 0.2, 0.1 and -0.1. The positive regions are shaded. The coordinates are measured in terms of the grid size so that the unit on the horizontal axis is double that on the vertical one.

These two correlation functions exhibit globally the same behaviour in the development of the oblique structure of the flow field. The direction of the longest correlation is initially inclined at 45° to the downstream. They are more and more inclined toward the streamwise direction, but eventually the inclination angle seems to stay at around some equilibrium value. The correlation function of ω_3 is very thin and long, which is characteristic of the structure of vortex layers (§4.2). Incidentally, the form of the correlation function of the magnitude of vorticity ($|\boldsymbol{\omega}| - \langle|\boldsymbol{\omega}|\rangle$) is similar to that of the transverse component (figures omitted).

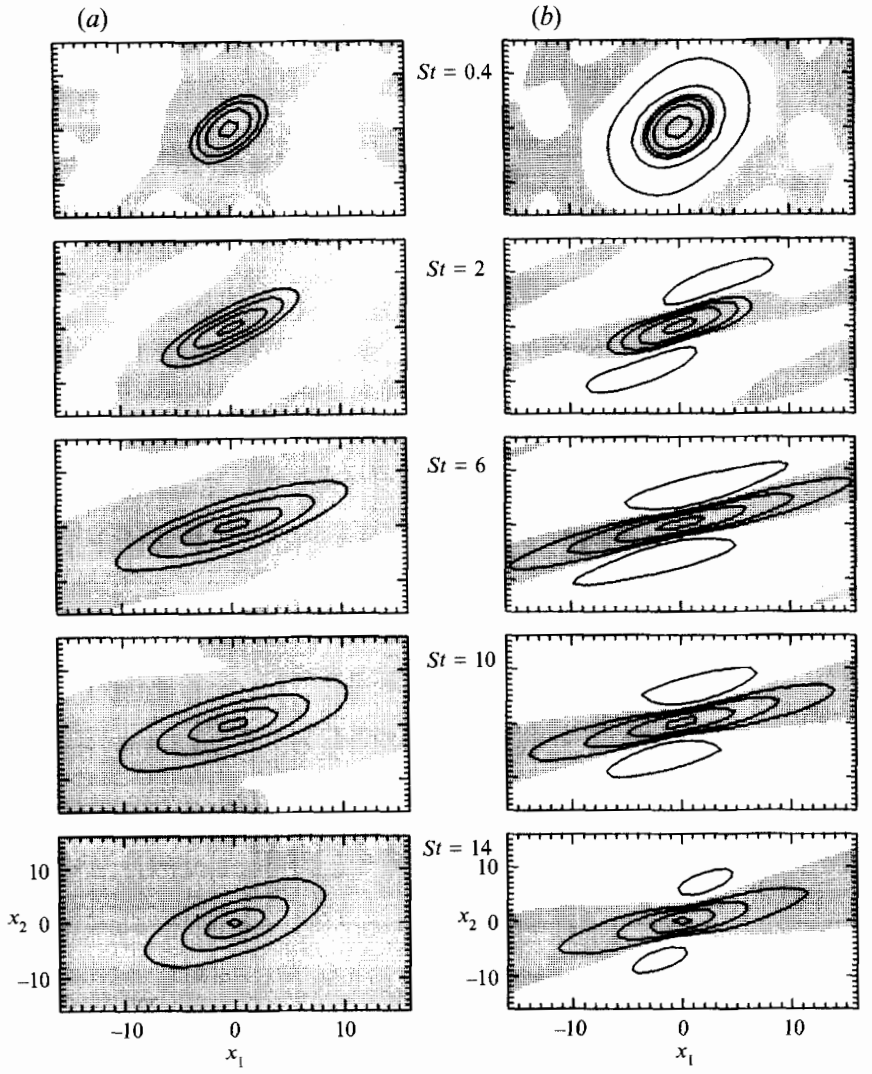

FIGURE 8. Time-evolution of two-point correlation functions in the transverse (x_1, x_2)-plane of (*a*) the transverse component $(\omega_1^2+\omega_2^2)^{1/2}-\langle(\omega_1^2+\omega_2^2)^{1/2}\rangle$ and (*b*) the spanwise component ω_3. They take a maximum value at the origin which is normalized to be unity. Contour levels are 0.8, 0.4, 0.2, 0.1, −0.1. Positive regions are shaded.

In order to discuss the oblique structure quantitatively we introduce the angles of direction of maximum correlations of the vorticity components. The angles of strong correlations for $(\omega_1^2+\omega_2^2)^{1/2}$, ω_3 and $|\boldsymbol{\omega}|$ are denoted by $\theta_{1,2}$, θ_3, $\theta_{|\omega|}$, respectively. Their time evolutions are plotted in figure 9(*a*) by filled symbols. They start at 45° and decrease monotonically to around 10°–20°, which is close to 22°, the value observed by Rogers & Moin (1987). Since $(\omega_1^2+\omega_2^2)^{1/2}$ is dominant at the initial period and ω_3 at later period, the angle $\theta_{|\omega|}$ is close to $\theta_{1,2}$ at earlier times but close to θ_3 at later times. Note here that these angles were determined by inspection of the contours of the correlation functions and there is ambiguity of about $\pm 2°$.

As will be discussed in the next section, the orientations of flow structure and the vorticity vector should be distinguished in considering the dynamics of vortical

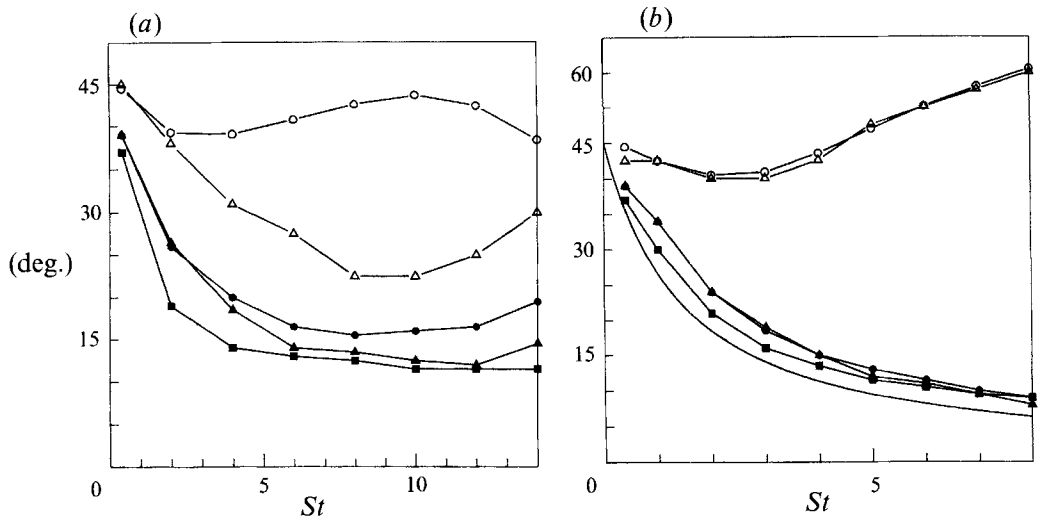

FIGURE 9. Time-evolution of various inclination angles: ○, $\theta_{\omega\omega}$, inclination angle of the principal axis of $\langle\omega_i\omega_j\rangle$ $(i,j=1,2)$; △, θ_{peak}, angle of longitudinal vortex tubes to the (x_2, x_3)-plane; ●, $\theta_{1,2}$, inclination angle of direction of strong correlation of $(\omega_1^2+\omega_2^2)^{1/2}-\langle(\omega_1^2+\omega_2^2)^{1/2}\rangle$; ▲, $\theta_{|\omega|}$, that of $(|\omega|-\langle|\omega|\rangle)$; ■, θ_3, that of ω_3. (*a*) Full Navier–Stokes calculation. (*b*) Rapid distortion calculation. Solid curve represents the analytical result of $\theta=\arctan(1/(1+St))$ in the rapid distortion approximation.

structures. Strong correlation angles $\theta_{1,2}$, θ_3 and $\theta_{|\omega|}$ may be good indicators of the orientation of stripe structure of the flow field. On the other hand, there are two angles that may represent the mean direction of vorticity vectors. One is the inclination angle $\theta_{\omega\omega}$ of the principal axis of the second-order moment of vorticity $\langle\omega_i\omega_j\rangle$ $(i,j=1,2)$, that is $\theta_{\omega\omega}=\frac{1}{2}\arctan[2\langle\omega_1\omega_2\rangle/(\langle\omega_1^2\rangle-\langle\omega_2^2\rangle)]$. The other is the angle θ_{peak} of longitudinal vortices to the (x_2, x_3)-plane, that is $\theta_{peak}=\arctan(\operatorname{cosec}\beta_{peak}\tan\alpha_{peak})$. These angles are plotted by open symbols (○ for $\theta_{\omega\omega}$ and △ for θ_{peak}) in figure 9(*a*). It is evident that these angles of the vorticity vectors are much larger than those of flow structures. In particular, the inclination angle $\theta_{\omega\omega}$ is remarkably large (around 40°). This is because wavy vortex layers (§4.2) yield large values of ω_2 in addition to the deviation of vorticity vectors from the structure (§4.1). A similar behaviour of these angles was observed in their high-Reynolds-number shear case by Rogers & Moin (1987).

For comparison, we show in figure 9(*b*) the time evolution of the above angles in a rapid distortion calculation. The correlation angles, $\theta_{1,2}$, θ_3, and $\theta_{|\omega|}$, decrease monotonically in time, while the vorticity angles, $\theta_{\omega\omega}$ and θ_{peak}, increase after a transient period ($St\lesssim 2$). None of these angles seem to approach any equilibrium value. This indicates that the linear mean shear is sufficient to make the vortical structure incline to the downstream whereas the vorticity vectors deviate in the opposite direction. The solid curve represents the analytical expression $\theta=\arctan(1/(1+St))$ in rapid distortion theory. The almost identical change in time of each group of angles suggests that the flow structure in the linear case is quite simple.

For later convenience, we introduce a new coordinate system (x_s, x_n, x_3) along the oblique structure of the flow (figure 10). Here, we take $\theta_{1,2}$ as the structure angle. We call the x_s- and x_n-axes the structural and normal directions, respectively.

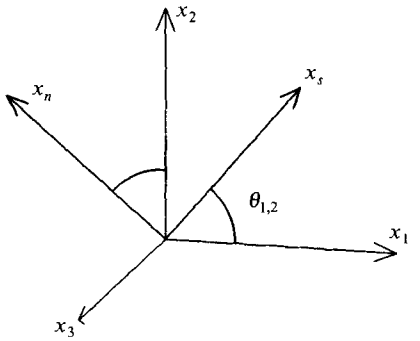

FIGURE 10. Structural coordinate system (x_s, x_n, x_3).

4. Dynamics of vortical structures

4.1. *Longitudinal vortex tubes*

As described in the preceding section, longitudinal vortex tubes are born at the initial period in directions 45° and 225° to the downstream, and incline, as the flow develops, more and more to the mean-stream axis, i.e. the vertical peak angle α_{peak} of fluctuating vorticity vector in longitudinal vortex tubes moves toward 0°. On the other hand, the horizontal peak angle β_{peak} moves toward $\pm 180°$ (against the mean vorticity). The angle β^T_{peak} for the total vorticity seems to stay at around $\pm 90°$ at later times. Here we consider a mechanism for this behaviour of the vorticity vectors.

The decrease of the vertical peak angle α_{peak} may be understood more easily with reference to the vorticity equation (2.3). The first term in the second brackets of (2.3) represents a conversion of the vertical component of vorticity to the streamwise one by the mean linear shear. The rate of change in time of this conversion is proportional to the vertical component. For an isotropically distributed vorticity field vorticity vectors with angles 45° and 225° to the downstream will be stretched most effectively by this conversion term. Recall that the first term in the first brackets in (2.3) represents an inclination of the flow structure by the linear shear. Therefore, if vorticity vectors are aligned along a straight line at some instant of time, they continue to be inclined along the direction of the aligned line (figure 11). Only these two terms would make a vortex tube incline to the downstream with vorticity aligning along it.

As the flow develops, a vorticity blob is elongated more and more by the above stretching process. Meanwhile, a vortex blob with initially relatively high vorticity develops into an elongated thin vortex blob with stronger vorticity. If the net vertical component of vorticity inside the blob is positive, then the vorticity vectors tend to point up and to the right as shown in figure 12(*a–c*). On the other hand, if it is negative, the vorticity vectors tend to point down-left as shown in figure 12(*d–f*). An elongated vorticity blob with high vorticity (now called a vortex tube) induces a strong swirling motion around it. The second term in the second brackets in (2.3), which is also linear in fluctuations and represents a conversion of the mean vorticity $(-S)$ into the direction of the spanwise derivative of the fluctuating velocity $\partial \boldsymbol{u}/\partial x_3$, begins to take part in the dynamics. In figure 12(*b, c, e, f*), the directions of velocity induced by vortex tubes are shown by curved arrows. It is evident that the spanwise derivative of this induced velocity is directed as shown with the big open arrows, which turns the vorticity vectors as shown with broken arrows in the figures. As a result, it retards the leaning toward the streamwise direction of the vorticity vectors compared with that of

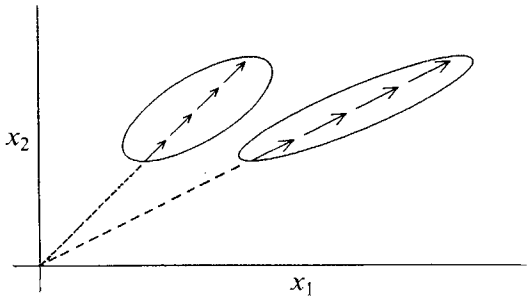

FIGURE 11. Vortical structure (bounded by a curve) and vorticity vectors (denoted by arrows) are inclined at the same rate.

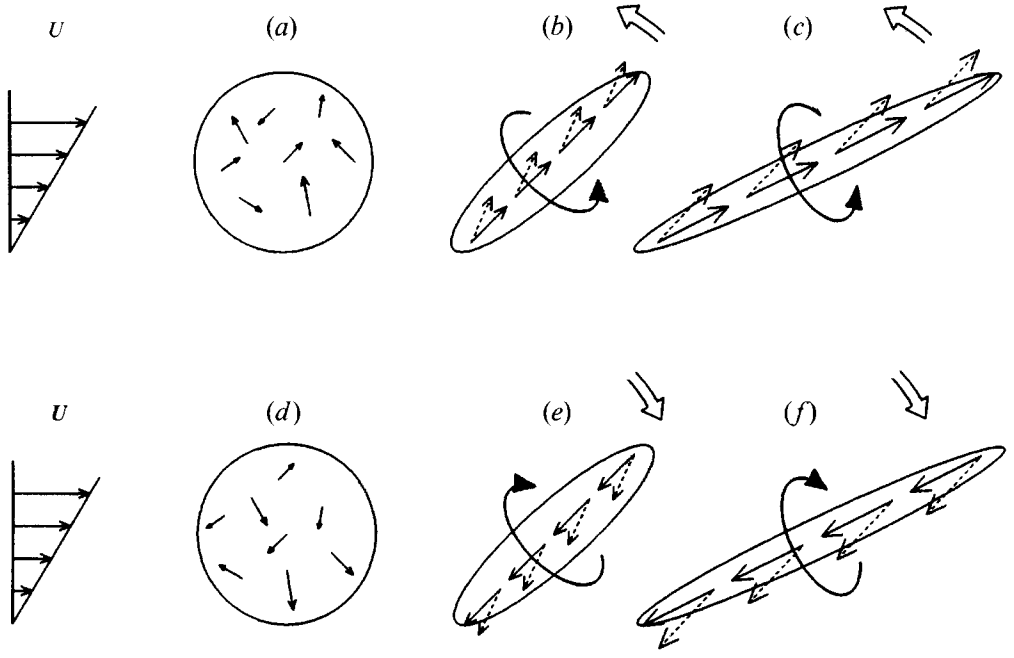

FIGURE 12. Deviation in orientation between a longitudinal vortex tube and the vorticity vectors therein. Net vertical vorticity is positive in (a, b, c), while it is negative in (d, e, f). Time elapses from (a) to (c) and from (d) to (f). Solid and broken straight arrows denote the vorticity vectors, and curved arrows show the direction of velocity induced by elongated vortex tubes. Big open arrows denote vorticity converted from the mean vorticity.

the vortex tube itself *irrespective* of the direction of vorticity vector. Thus, a deviation inevitably appears in the direction of the longitudinal vortex tubes and vorticity vectors therein. This deviation in turn causes a horizontal turning of the vorticity vectors (see below). So far, we have found that both the transverse components, ω_1 and ω_2, increase in strength, the former being larger than the latter. The spanwise component ω_3, on the other hand, does not show any rapid growth because there is no stretching in this direction by the mean shear. Hence, the ordering $v_{11} > v_{22} > v_{33}$ holds at the initial stage of evolution (figure 2).

In order to check whether the above mechanism is actually taking place, we estimate

St	2	6	14
$(\hat{x}_n \cdot \hat{x}_1) S\omega_2$	0.00 ($\mp$5.35)	0.00 ($\mp$2.96)	0.00 ($\mp$6.35)
$\omega_s \partial u_n/\partial x_s$	0.01 ($\pm$0.56)	0.00 ($\mp$0.14)	0.01 ($\pm$0.67)
$\omega_n \partial u_n/\partial x_n$	−0.01 ($\mp$0.20)	0.05 ($\mp$0.17)	−0.03 ($\mp$0.53)
$(\omega_3 - S)\partial u_n/\partial x_3$	−0.01 ($\pm$3.00)	−0.06 ($\pm$0.60)	0.03 ($\pm$0.54)
$\nu\nabla^2\omega_n$	0.00 ($\mp$0.33)	0.00 ($\pm$0.28)	0.00 ($\pm$0.80)
$D\omega_n/Dt$	0.00 ($\mp$2.32)	0.00 ($\mp$2.39)	0.00 ($\mp$4.87)

TABLE 1. Contribution to $D\omega_n/Dt$ from each term on the right-hand side of (4.1). The averages over the whole space and over tube regions (in brackets) are shown. The figures are multiplied by 0.1. Tube regions are defined as $|\alpha \mp 37.5°| \leqslant 12.5°$, $|\beta \mp 105°| \leqslant 25°$ (415146 points) at $St = 2$; $|\alpha^T \mp 27.5°| \leqslant 12.5°$, $|\beta^T \mp 90°| \leqslant 30°$ (302601 points) at $St = 6$; $|\alpha^T \mp 27.5°| \leqslant 12.5°$, $|\beta^T \mp 90°| \leqslant 30°$ (305096 points) at $St = 14$. Number of total points is 128^3 (= 2097152). Inclination angle of $\hat{x}_s$ to $\hat{x}_1$ is 25°, 15° and 20° at $St = 2$, 6 and 14, respectively. The upper and lower signs refer to the longitudinal vortex tubes with downward and upward vorticity, respectively.

the contribution of each term in (2.3) to the change in time of the normal component ω_n of vorticity by rewriting the equation as

$$\frac{D\omega_n}{Dt} \equiv \frac{\partial \omega_n}{\partial t} + \left(Sx_2 \frac{\partial \omega_n}{\partial x_1} + u_j \frac{\partial \omega_n}{\partial x_j} \right)$$

$$= (\hat{x}_n \cdot \hat{x}_1) S\omega_2 + \omega_s \frac{\partial u_n}{\partial x_s} + \omega_n \frac{\partial u_n}{\partial x_n} + (\omega_3 - S) \frac{\partial u_n}{\partial x_3} + \nu\nabla^2\omega_n, \tag{4.1}$$

where $\hat{x}_n$ is the unit vector in the normal direction.

To estimate the magnitude of each term for longitudinal vortex tubes, we calculated their mean values over those grid points on which the orientation angles (α, β) or (α^T, β^T) are close to the peak values corresponding to longitudinal vortex tubes. We took rectangular regions of $|\alpha \mp 37.5°| \leqslant 12.5°$, $|\beta \pm 105°| \leqslant 25°$ at $St = 2$, $|\alpha^T \mp 27.5°| \leqslant 12.5°$, $|\beta^T \pm 90°| \leqslant 30°$ at $St = 6$, and $|\alpha^T \mp 27.5°| \leqslant 12.5°$, $|\beta^T \pm 90°| \leqslant 30°$ at $St = 14$. The results are shown in brackets in table 1. The upper and lower signs correspond to longitudinal vortex tubes with vorticity directed downstream and upstream, respectively. Conversion of vorticity by the mean shear $(\hat{x}_n \cdot \hat{x}_1) S\omega_2$ is always dominant so that the vorticity vectors are inclined more and more toward the streamwise direction (figure 7*b*). Conversion of vorticity from the spanwise component $(\omega_3 - S)\partial u_n/\partial x_3$ takes large values at early times ($St = 2$), as expected from the above discussion.

The deviation mechanism described above is due to the direct interaction of the fluctuating vorticity and the mean shear. The effects of this interaction are clearly observed in a rapid distortion field. As seen in figure 9(*b*), the vorticity angles are much larger than the structural angles. In figure 13(*a*) we show the high-vorticity regions (longitudinal vortex tubes) at $St = 4$ shadowed and vorticity vectors by lines with arrows indicating the direction in the transverse (x_1, x_2)-plane. It is evident that the vorticity vectors (inclined at 40°–42° are much steeper than the vortex tubes (inclined at 14°–15°) and that the vorticity lines penetrate the iso-surfaces of vorticity. It should be remembered here that the vorticity does not change abruptly on these iso-surfaces, but rather it is distributed continuously in space. Thus, the penetration of vorticity vectors through the iso-surface does not violate the solenoidal condition of vorticity.

The vorticity distribution in a plane (x_3, x_n) perpendicular to the structural direction which is inclined at 15° to the downstream is shown in figure 13(*b*) (plate 1). This is a

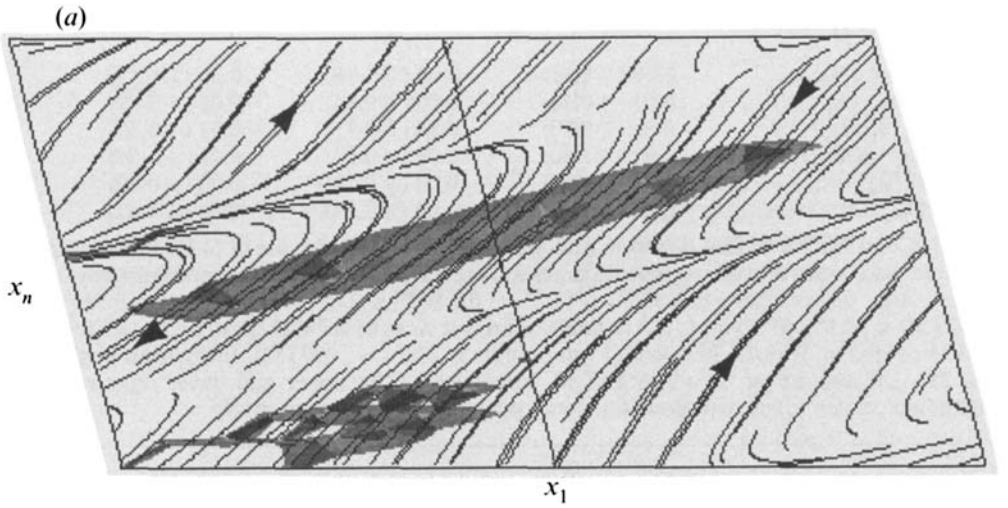

FIGURE 13. (*a*) High-vorticity region (shaded) and vorticity vectors (lines with arrows) seen from the spanwise direction at $St = 4$ in a rapid distortion calculation in $6 \leqslant x_1'/\Delta x_1 \leqslant 22$, $27 \leqslant x_2/\Delta x_2 \leqslant 43$, $39 \leqslant x_3/\Delta x_3 \leqslant 53$, where $x_1' = x_1 + (\tan 15°)\, x_2$. (*b*, plate 1) Vorticity field on a plane perpendicular to the structure (inclined at 15° to the downstream). Rapid distortion calculation. $St = 4$. The structural component ω_s is represented by a colour map ($-2.5S$ (blue) $\leqslant \omega_s \leqslant 2.5S$ (red)). Red and blue regions are rotating in clockwise and counterclockwise directions, respectively. White lines represent the perpendicular component (ω_3, ω_n) which points upward (downward) in red (blue) regions. $-3.7S \leqslant \omega_s \leqslant 3.4S$, $-1.7S \leqslant \omega_n \leqslant 1.6S$, $-2.8S \leqslant \omega_3 \leqslant 2.4S$. $x_1' = 14\Delta x_1$, $27 \leqslant x_2/\Delta x_2 \leqslant 43$, $25 \leqslant x_3/\Delta x_3 \leqslant 54$. (*c*, plate 1) Same as (*b*) but for the full Navier–Stokes calculation at $St = 4$ continued from a rapid distortion field at $St = 3$. The perpendicular component of vorticity is inclined to the right in both the red and blue regions. There is a strong vortex layer extending horizontally at the lower centre. $-3.3S \leqslant \omega_s \leqslant 3.1S$, $-1.8S \leqslant \omega_n \leqslant 1.4S$, $-4.9S \leqslant \omega_3 \leqslant 2.8S$.

cross-section of figure 13(*a*). The structural component ω_s is represented by a colour map, with red and blue representing clockwise and counterclockwise rotation, and the perpendicular component (ω_3, ω_n) represented by white lines. Inside of vortex tubes the normal component ω_n is positive (negative) in regions of $\omega_s > 0$ ($\omega_s < 0$) though the direction is not shown explicitly. The mean flow is into the page. As stated above, the vorticity lines penetrate the boundary of the vortex tubes. This behaviour is typical and commonly observed in the whole field.

Next, we consider the change in time of the horizontal angle β_{peak}. This is certainly caused by the nonlinear mechanism because we confirmed that β_{peak} stays at $\pm 90°$ in the rapid distortion calculation. The following is an explanation of the change of β_{peak}, i.e. a turning of longitudinal vortex tubes against the mean vorticity.

The spanwise component of (2.3) is written as

$$\frac{\mathrm{D}\omega_3}{\mathrm{D}t} = \omega_s \frac{\partial u_3}{\partial x_s} + \omega_n \frac{\partial u_3}{\partial x_n} + (\omega_3 - S)\frac{\partial u_3}{\partial x_3} + \nu \nabla^2 \omega_3. \tag{4.2}$$

The first two terms on the right-hand side of (4.2) represent respectively conversions of ω_s and ω_n to the spanwise component by the fluctuating velocity field, whereas the third one is a contribution from the spanwise stretching. The magnitude of each of these terms may be estimated by taking into account of deviation in direction between longitudinal vortex tubes and the vorticity vectors therein. Figure 14 shows a longitudinal vortex tube with vorticity directed (*a*) downstream and (*b*) upstream.

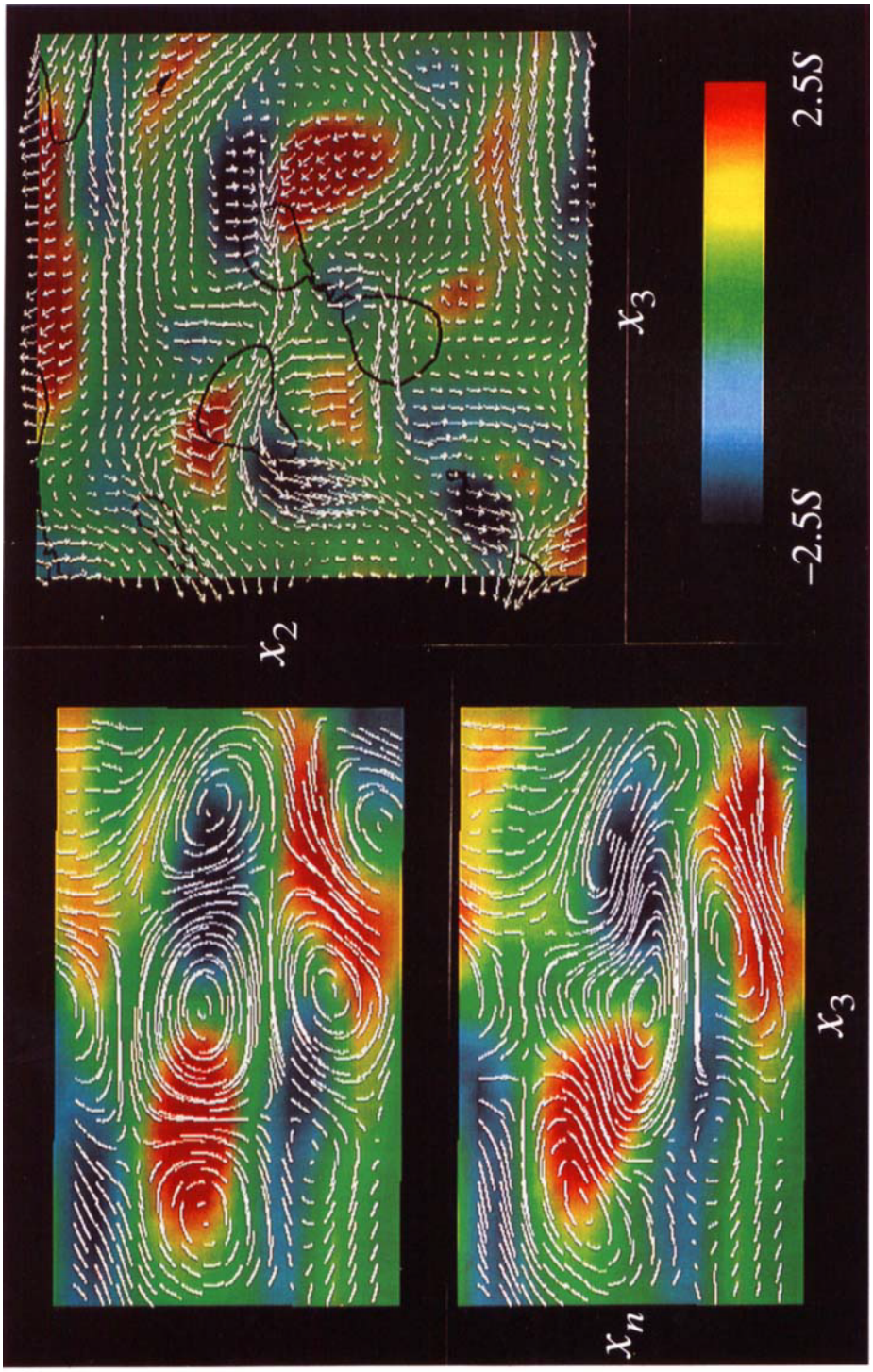

FIGURE 13(*b*, *c*). For caption see figure 13(*a*).

FIGURE 17(*a*). For caption see figure 17 (*b*)

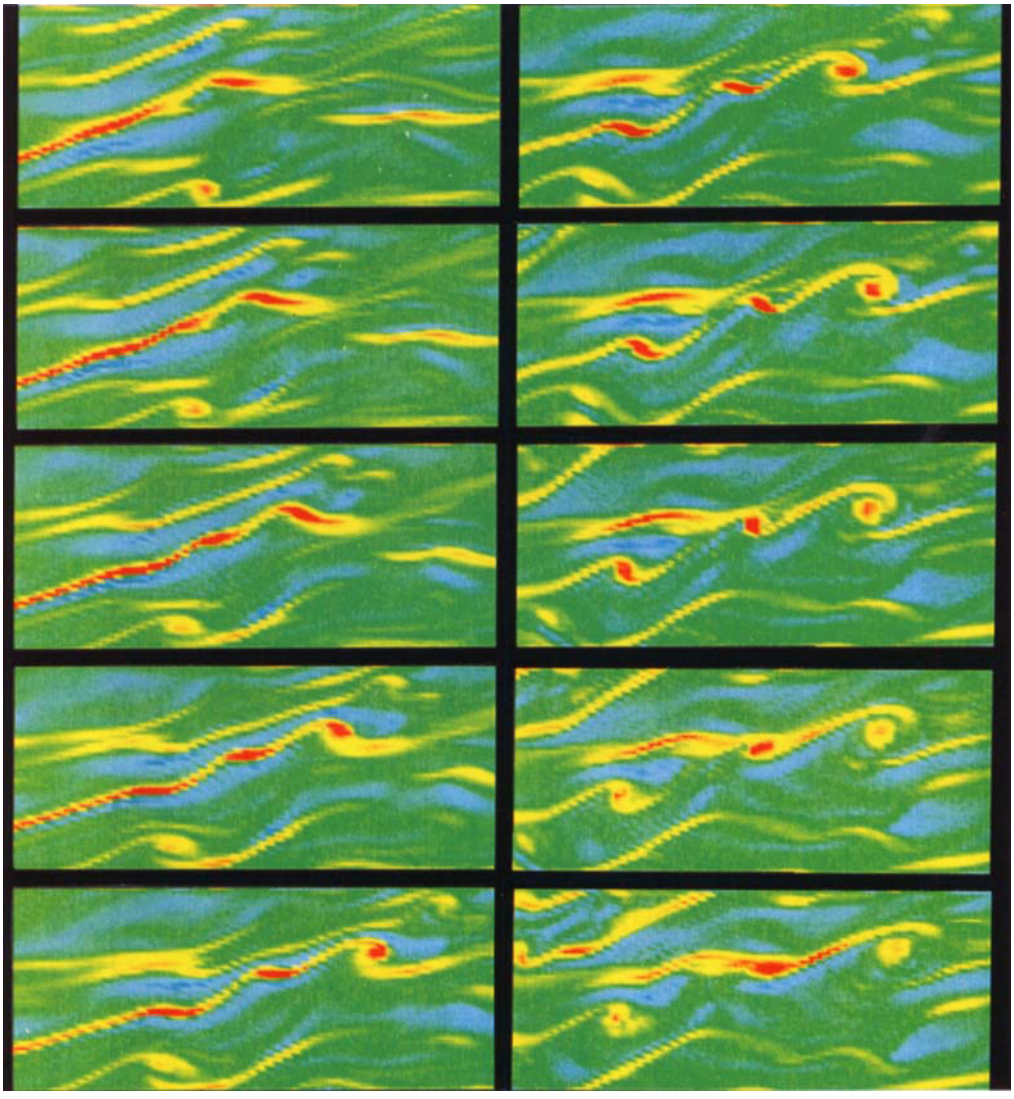

FIGURE 19. Rolling-up of vortex layers. Spanwise vorticity ω_3 is drawn in the (x_1, x_2)-plane. Red and blue denote negative and positive values, respectively. St = 8.8, 9.2, 9.6, · · ·, 12.4.

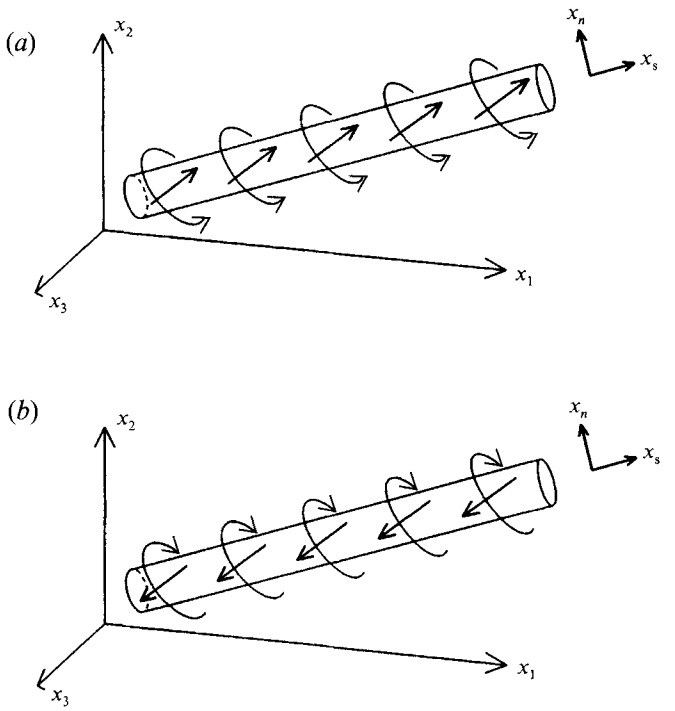

FIGURE 14. The turning toward the positive x_3-direction of the vorticity vectors in a longitudinal vortex tube with vorticity directed (*a*) downstream and (*b*) upstream. Straight arrows denote vorticity vectors, and curved arrows show the direction of velocity induced by the vortex tubes. In both cases $\omega_n \partial u_3/\partial x_n$ gives a positive contribution.

St	2	6	14
$\omega_s \partial u_3/\partial x_s$	−0.14 (−0.80, 0.06)	−0.05 (−0.33, 0.09)	0.01 (−1.68, −0.54)
$\omega_n \partial u_3/\partial x_n$	0.73 (3.33, −0.48)	1.27 (4.19, 0.57)	1.60 (6.26, −2.34)
$(\omega_3 - S)\partial u_3/\partial x_3$	−0.59 (−0.49, −4.52)	−1.22 (−0.19, −3.60)	−1.60 (−0.46, −8.04)
$\nu\nabla^2\omega_3$	0.00 (−1.11, 2.98)	0.00 (−3.71, 2.70)	0.00 (−4.62, 7.10)
$D\omega_3/Dt$	0.00 (0.93, −1.96)	0.00 (−0.04, −1.56)	0.01 (−0.50, −3.86)

TABLE 2. Contribution to $D\omega_3/Dt$ from each term on the right-hand side of (4.2). The averages over the whole space, over tube regions (the first number in brackets) and over layer regions (the second number in brackets) are shown. The numbers are multiplied by 0.1. Tube regions are the same as those in table 1. Layer regions are defined as $|\alpha| \leqslant 40°$, $|\beta| \leqslant 30°$ (180250 points) at $St = 2$; $|\alpha^T| \leqslant 35°$, $|\beta^T| \leqslant 30°$ (771886 points) at $St = 6$; $|\alpha^T| \leqslant 40°$, $|\beta^T| \leqslant 30°$ (517917 points) at $St = 14$. Inclination angle of $\hat{\boldsymbol{x}}_s$ to $\hat{\boldsymbol{x}}_1$ is 25°, 15° and 20° at $St = 2$, 6 and 14, respectively.

(Again recall that vorticity is distributed outside the tubes too.) The straight arrows denote the direction of vorticity vectors inside the vortex tube. Vorticity vectors are inclined to the downstream less than the vortex tube itself. Curved arrows denote the direction of rotation of the vorticity field around the vortex tube. It is seen in these figures that $\omega_n \partial u_3/\partial x_n$ gives a positive contribution in both cases. This explains the turning of the vorticity vectors toward the positive x_3-axis (against the mean vorticity). Note that this is a result of nonlinear interactions which are neglected in the rapid distortion calculation. Incidentally, the same argument may apply to show that the vorticity vectors in a vortex tube rotate around the axis of the tube if its vorticity is

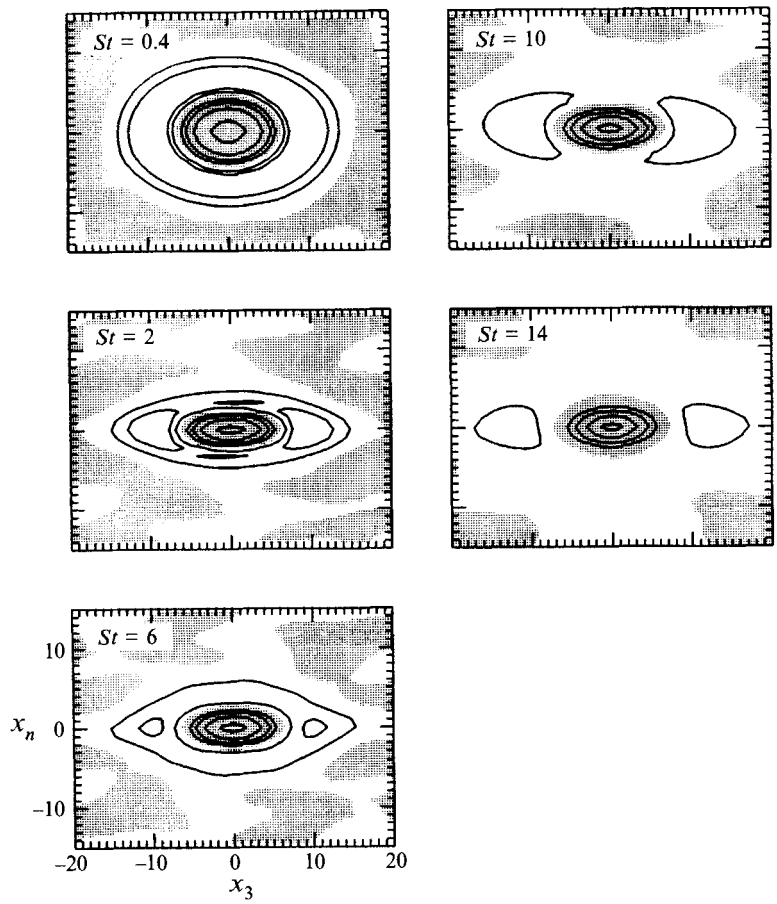

FIGURE 15. Correlation function of vorticity components in the direction of θ_{peak} on the (x_3, x_n)-plane. The value at the origin is normalized to be unity. Contour levels are 0.8, 0.4, 0.2, 0.1, −0.025, −0.05, −0.1. Positive regions are shaded.

strong enough for the nonlinear interaction to play a role, that is the direction of vorticity vectors has a tendency to stay near that of vortex tubes.

The relative magnitude of each term in (4.2) in longitudinal vortex tubes is estimated in our numerical turbulence in the same way as in (4.1). The results are shown as the first number in brackets in table 2. It is seen that the contribution from $\omega_n \partial u_3/\partial x_n$ is actually large at all three time instants. The contribution from the other nonlinear terms is quite small. The viscous diffusion works against the increase of ω_3 at the two later times. The Lagrangian derivative $D\omega_3/Dt$ is positive at $St = 2$, meaning that vorticity vectors inside longitudinal vortex tubes are turning toward the positive x_3-axis. The derivative takes small negative values at $St = 6$, suggesting that the horizontal peak angle β_{peak} is already in equilibrium by this time. It is not clear to us why β^T stays at around $\pm 90°$ at later times (figure 6*b*).

In order to substantiate the above scenario of turning of vorticity vectors, we integrated the rapid distortion field at $St = 3$ further using the full Navier–Stokes equation. The vorticity field thus obtained at $St = 4$ is shown in figure 13(*c*) (plate 1). It is clearly seen that the vorticity vectors inside vortex tubes are turned toward the positive x_3 axis.

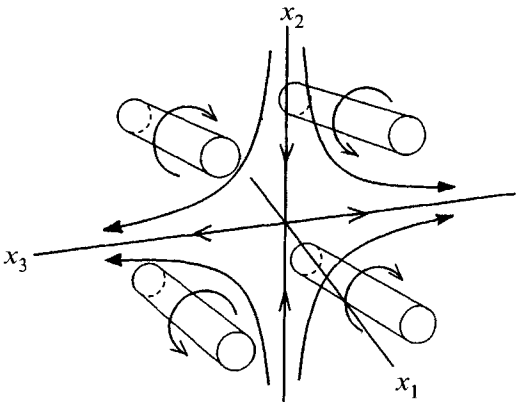

FIGURE 16. Mechanism for the generation of a vortex layer. If two pairs of longitudinal vortex tubes are arranged as in this figure, they stretch vorticity lines to generate a vortex layer in the x_3-direction. Arrows indicate the direction of velocity induced by the vortex tubes.

By comparing several realizations with different initial spectra of the velocity field of the form (2.9) with various values of c and k_0, we found that the mutual distance among longitudinal vortex tubes at early times is determined by the lengthscale ($\sim 2\pi/k_0 \approx 7\Delta x_3$) of the initial distribution of vorticity. Figure 15 shows the two-point correlation function of vorticity components in the direction of θ_{peak} on a plane normal to the structural direction. The correlation length in the spanwise direction is invariant in time, staying at around 10 mesh sizes. But the length in the normal direction decreases in time to a few mesh sizes. This is caused by distortion due to the linear mean shear. The shrinking of the lengthscale in the normal direction enhances stretching by longitudinal vortex tubes in the spanwise direction (see figure 17 below).

As expected from the rather complicated structures of high-vorticity regions shown in figure 3, the motion of longitudinal vortex tubes is not so simple. In fact, individual vortex tubes are hardly straight but change their shape flabbily. The orientation of the tubes inclines more and more on average and approaches the streamwise direction. The intensity tends to decrease for the more inclined parts of tubes. But parts of tubes that happen to have a larger angle to the streamwise direction get more effective stretching to grow into intensified longitudinal vortex tubes. As discussed in §3.2 with reference to figure 7(*b*), vorticity is supplied from vortex layers to longitudinal vortex tubes through wrapping or entraining (see also §4.2). The peak orientation angles $(\alpha^T_{peak}, \beta^T_{peak}) = \pm(30°, 90°)$ of the vorticity vectors seem to be determined by the combined effects of many of these complicated dynamical processes.

4.2. *Vortex layers*

In the middle stage of evolution ($6 \lesssim St \lesssim 12$) layer-like structures are observed in the iso-vorticity surfaces (figures 3(*d*, *e*) and 4). We consider here a mechanism for generation of vortex layers.

Longitudinal vortex tubes, as discussed in §4.1, induce straining flows perpendicular to themselves. These straining flows distort the vorticity field in a somewhat random way, which on average stretches fluid elements. Since the spanwise component of vorticity of the mean shear dominates the other components, the stretching in the spanwise direction may most effectively contribute to magnify vorticity. Indeed a single vortex or a pair of vortices can generate shear flows, but an extremely strong shear flow

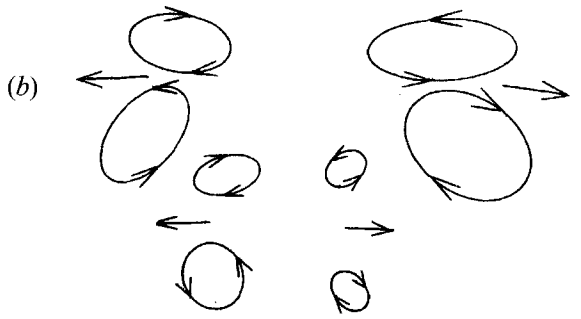

FIGURE 17. Spatial structure of the vorticity and spanwise velocity gradient in an (x_2, x_3)-plane at $St = 4$. (*a*, plate 1) The spatial distribution of streamwise vorticity ω_1 is shown with colour map in which red and blue regions rotate in clockwise and counterclockwise directions, respectively. The perpendicular components of vorticity (ω_3, ω_2) are shown by arrows. Strong spanwise expansion regions $(\partial u_3/\partial x_3 > 0.5S)$ are enclosed by black lines. $-3.8S \leqslant \omega_1 \leqslant 3.7S$, $-3.0S \leqslant \omega_2 \leqslant 2.2S$, $-2.2S \leqslant \omega_3 \leqslant 2.0S$. (*b*) Eight vortices (four pairs of vortices of opposite sign). Arrows on curves denote the direction of rotation of the vortices. Straight arrows denote the direction of translation of the vortex pairs. $x_1' = 16\Delta x_1$, $23 \leqslant x_2/\Delta x_2 \leqslant 55$, $95 \leqslant x_3/\Delta x_3 \leqslant 127$.

can be generated more effectively by the combined effects of two pairs of vortex tubes arranged as shown schematically in figure 16. If they happen to be arranged as shown in this figure, a strong vortex layer with a spanwise component of vorticity is generated between them.

In figure 17, we show the structure of vorticity field in an (x_2, x_3)-plane at $St = 4$. The mesh size of the plane is 32×32 $(23 \leqslant x_2/\Delta x_2 \leqslant 55,\ 95 \leqslant x_3/\Delta x_3 \leqslant 127)$. The spatial distribution of ω_1 is drawn in figure 17(*a*) (plate 1) with colour map in which red and blue denote clockwise and counterclockwise rotations, respectively. Among others, eight vortices (four pairs of vortices of opposite sign) are noticeable as sketched in figure 17(*b*). The left-hand pairs move to the left and the right-hand pairs move to the right. The transverse components of vorticity (ω_3, ω_2) are shown by arrows. Domains enclosed by black lines represent the regions of strong spanwise expansion $(\partial u_3/\partial x_3 > 0.5S)$. These regions of strong spanwise expansion appear behind each pair of vortices at which strong spanwise vortex layers in the direction of the mean vorticity (pointing to the left) are generated (see the three enclosed regions around the centre). It is interesting to recall that the direction of vorticity in vortex layers is opposite to that of turning of longitudinal vortex tubes (§3.3).

A blue region with downward arrows at the middle-left represents a downward longitudinal vortex tube which connects with a horizontal vortex layer on the right. This is a typical example of the interaction between vortex layers and longitudinal vortex tubes, which are observed here and there in the whole flow field. Tracking these interactions in a three-dimensional visualization, we observed that vortex layers are being either wrapped or entrained into longitudinal vortex tubes. The spanwise component of vorticity is transferred to the streamwise component by this process (see figure 7*b*) (cf. Jiménez & Moin 1991). A further investigation is necessary to make this mechanism clearer.

Each term in (4.2) which contributes to the change over time of the spanwise vorticity from vortex layers is shown as the second number in brackets in table 2. We see that $(\omega_3 - S)\partial u_3/\partial x_3$ actually gives a dominant contribution to the increase of negative spanwise vorticity at three times, $St = 2$, 6 and 14. Viscous diffusion works to opposite it.

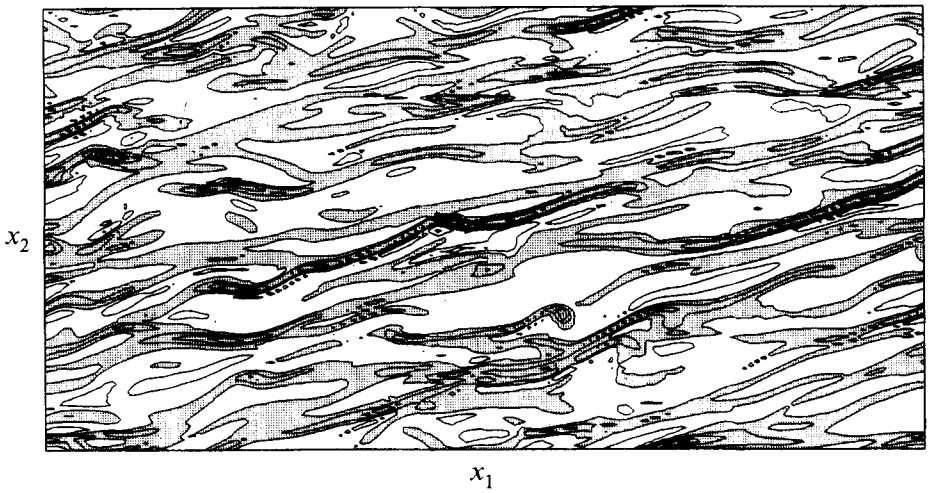

FIGURE 18. Contours of spanwise vorticity ω_3 on a plane $x_3 = 72\Delta x_3$ at $St = 9.2$. $0 \leqslant x_1/\Delta x_1$, $x_2/\Delta x_2 \leqslant 127$. Contour levels are 0, $\pm 1.5S$, $\pm 3S$, ... Negative regions are shaded. An oblique stripe structure which is inclined at 10°–20° to the downstream is evident.

In figure 18, we draw contours of the spanwise vorticity on the plane $x_3 = 72$ at $St = 9.2$. The domain is the whole simulated region in the (x_1, x_2)-plane. The existence of an oblique stripe structure inclined by 10°–20° to the downstream is evident (§3.3). These elongated thin vortical structures are actually vortex layers. Their length covers typically several tens of mesh sizes, their thickness a few mesh sizes, and their width nearly ten mesh sizes.

4.3. *Lateral vortex tubes*

Vortex layers, which are described in the preceding section, are rolled up into lateral vortex tubes typically by the Kelvin–Helmholtz instability (Ruetsch & Maxey 1992). Figure 19 (plate 2) is a time series of the spanwise component of vorticity on the (x_1, x_2)-plane when a thin vortex layer rolls up to make vortex tubes. Colour represents the value of the spanwise component of vorticity; red is for clockwise rotation and blue for counterclockwise rotation. A rolling-up process of a vortex layer into three well-defined vortex tubes is clearly seen. This is the Kelvin–Helmholtz instability. The thin layer shown in figure 19 covers a few meshes widths so that the half-width δ is estimated to be $(2\pi/128) \times 2 \approx 0.1$. Half of the velocity difference U_0 across the layer is about 9. Hence, the relevant Reynolds number is $Re = U_0\,\delta/\nu = 90$. There are about 12 meshes in the x_1-direction between adjacent vortex tubes so that the distance λ is estimated to be $(4\pi/128) \times 12 \approx 1.2$. The linear stability of a unidirectional shear flow of tanh-type, $U = U_0 \tanh y/\delta$, was investigated by Betchov & Szewczyk (1963). The wavelength λ of the most rapidly growing mode is about 14δ for $Re = 90$ (see figure 1 of their paper), which is comparable with the above numerical values.

Many strong lateral vortex tubes with high vorticity are always observed at the later stages of evolution. There may be other instability mechanisms than the Kelvin–Helmholtz one such as a generation mechanism of vortex tubes in a rotating flow (Hopfinger, Browand & Gagne 1982; Rogers & Moin 1987). These lateral vortex tubes are distorted by the random velocity field into longitudinal vortex tubes and complicated hairpin vortices which break down back into the random vorticity field (see Sandham & Kleiser 1992).

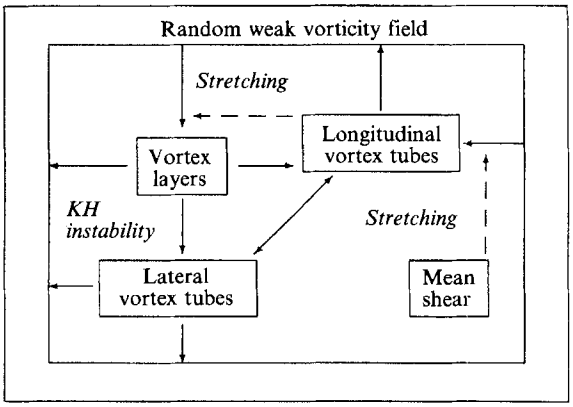

FIGURE 20. Formation and breakdown of the vortical structure in a uniform shear flow. The linear mean shear flow stretches a random vorticity field to generate longitudinal vortex tubes. Longitudinal vortex tubes induce swirling motion around them which stretches vorticity lines most effectively in the negative spanwise direction to generate vortex layers. Vortex layers roll up, through Kelvin–Helmholtz instability, into lateral vortex tubes. There are strong mutual interactions among longitudinal vortex tubes, lateral vortex tubes, vortex layers, and the linear mean shear. All of these typical structures break down into a disordered weak vorticity field through various instability mechanisms.

5. Concluding remarks

We have investigated the mechanism of generation and development of vortical structures in a homogeneous shear flow by analysing the results of direct numerical simulations of the Navier–Stokes equation. It was found that a few types of vortical structures dominate in a complicated fluctuating vorticity field. They are *longitudinal vortex tubes*, which are orthogonal to the spanwise direction and inclined at 15°–30° to the downstream, and *lateral vortex tubes* and *vortex layers* with spanwise vorticity.

We have observed the following scenario of generation, development and breakdown of vortical structures (figure 20).

(i) The linear mean shear flow stretches a randomly distributed initial vorticity field to generate many elongated vortex tubes, which we call *longitudinal vortex tubes*. The longitudinal vortex tubes are born perpendicularly to the spanwise direction and inclined at 45° and 225° to the downstream, which are the directions of maximal extension of the mean shear flow. The mutual distance between the longitudinal vortex tubes is determined by the lengthscale of the initial fluctuating vorticity. There seem to be no direct relations between the mutual distance and the mean shear rate, unlike the streak structure observed in turbulent boundary layers.

(ii) These longitudinal vortex tubes are subsequently inclined more and more toward the streamwise direction with further increase in their vorticity. Vorticity vectors inside longitudinal vortex tubes are less inclined (by about 10°) than the tubes themselves. That is, there is a substantial deviation in direction between the vortex tubes and vorticity vectors therein. Strong longitudinal vortex tubes induce strong swirling motion around them which stretches fluid elements in a somewhat random way. Because there is relatively high vorticity of the mean shear in the negative spanwise direction, stretching of fluid elements in the spanwise direction is more effective in increasing the spanwise component of vorticity. Then, *vortex layers* with a spanwise component of vorticity are generated along planes nearly parallel both to the longitudinal vortex tubes and to the spanwise axis.

(iii) These vortex layers roll up, through the Kelvin–Helmholtz instability, into vortex tubes in the spanwise direction, which is called the *lateral vortex tubes*. These lateral vortex tubes are stretched and distorted by the mean shear to make hairpin vortex tubes. There are also complicated three-dimensional interactions between vortex layers and longitudinal vortex tubes; the former are either wrapped or entrained into the latter. Moreover, there should be some interactions between longitudinal and lateral vortex tubes, though we have not identified any of them clearly yet.

(iv) All of these typical structures break down into a *disordered weak vorticity field* through various instability mechanisms and complicated mutual interactions.

(v) Owing to continuous distortion due to the linear mean shear, an oblique stripe structure, which inclines at 10°–15° to the downstream, prevails in the whole flow field. This leads to a suppression of fluctuations of velocity and vorticity in the vertical direction (see figure 3 in Kida & Tanaka 1992).

(vi) Since there is no characteristic length in homogeneous shear turbulence, the characteristic amplitude and length of the fluctuating flow field increase without limit. The turbulent energy, enstrophy, and Reynolds stress increase exponentially (Tavoularis 1985; Tavoularis & Karnik 1989; Kida & Tanaka 1992). But the flow structure develops statistically similarly, as do the dynamical processes among various vortical structures.

It is important to clarify how these vortical structures take part in turbulence dynamics, such as turbulent diffusion, mixing and transport of heat, mass, momentum and kinetic energy of fluid elements and contamination, production of turbulent energy, and so on. The study of such dynamical roles of vortical structures is currently under way and the results will be reported in a separate paper.

This work was partially supported by a Grant-in-Aid for Scientific Research from the Ministry of Education, Science and Culture.

REFERENCES

BETCHOV, R. & SZEWCZYK, A. 1963 Stability of a shear layer between parallel streams. *Phys. Fluids* **6**, 1391.

HOPFINGER, E. J., BROWAND, F. K. & GAGNE, Y. 1982 Turbulence and waves in a rotating tank. *J. Fluid Mech.* **125**, 505.

HOSOKAWA, I. & YAMAMOTO, K. 1989 Fine structure of a directly simulated isotropic turbulence. *J. Phys. Soc. Japan* **58**, 20.

HUSSAIN, A. K. M. F. 1986 Coherent structures and turbulence. *J. Fluid Mech.* **173**, 303.

JIMÉNEZ, J., COGOLLOS, M. & BERNAL, L. P. 1985 A perspective view of the plane mixing layer. *J. Fluid Mech.* **152**, 125.

JIMÉNEZ, J. & MOIN, P. 1991 The minimal flow unit in near-wall turbulence. *J. Fluid Mech.* **225**, 213.

KERR, R. M. 1985 Higher-order derivative correlations and the alignment of small-scale structures in isotropic numerical turbulence. *J. Fluid Mech.* **153**, 31.

KIDA, S. & TAKAOKA, M. 1994 Vortex reconnection. *Ann. Rev. Fluid Mech.* **26**, 169–189.

KIDA, S. & TANAKA, M. 1992 Reynolds stress and vortical structure in a uniformly sheared turbulence. *J. Phys. Soc. Japan* **61**, 4400.

KIDA, S. & TANAKA, M. 1993 Evolution of homogeneously sheared turbulence. In *Ninth Symp. on Turbulent Shear Flow*, p. 17–4–1. Kyoto.

KIM, J. & MOIN, P. 1986 The structure of vorticity field in turbulent channel flow. Part 2. Study of ensemble-averaged fields. *J. Fluid Mech.* **162**, 339.

KLINE, S. J., REYNOLDS, W. C., SCHRAUB, F. A. & RUNSTADLER, P. W. 1967 The structure of turbulent boundary layers. *J. Fluid Mech.* **30**, 741.

LEE, M. J., KIM, J. & MOIN, P. 1990 Structure of turbulence at high shear rate. *J. Fluid Mech.* **216**, 561.

ROGALLO, R. S. 1981 Numerical experiments in homogeneous turbulence. *NASA TM* 81315.

ROGERS, M. M. & MOIN, P. 1987 The structure of the vorticity field in homogeneous turbulent flows. *J. Fluid Mech.* **176**, 33.

RUETSCH, G. R. & MAXEY, M. R. 1992 The evolution of small-scale structures in homogeneous isotropic turbulence. *Phys. Fluids* A **4**, 2747.

SANDHAM, N. D. & KLEISER, L. 1992 The late stage of transition to turbulence in channel flow. *J. Fluid Mech.* **245**, 319.

SHE, Z.-S., JACKSON, E. & ORSZAG, S. A. 1990 Intermittent vortex structures in homogeneous isotropic turbulence. *Nature* **344**, 226.

SIGGIA, E. D. 1981 Numerical study of small-scale intermittency in three-dimensional turbulence. *J. Fluid Mech.* **107**, 375.

TANAKA, M. & KIDA, S. 1993 Characterization of vortex tubes and sheets. *Phys. Fluids* A **5**, 2079.

TAVOULARIS, S. 1985 Asymptotic laws for transversely homogeneous turbulent shear flows. *Phys. Fluids* **28**, 999.

TAVOULARIS, S. & KARNIK, U. 1989 Further experiments on the evolution of turbulent stresses and scales in uniformly sheared turbulence. *J. Fluid Mech.* **204**, 457.

TOWNSEND, A. A. 1970 Entrainment and the structure of turbulent flow. *J. Fluid Mech.* **41**, 13.

VINCENT, A. & MENEGUZZI, M. 1991 The spatial structure and statistical properties of homogeneous isotropic turbulence. *J. Fluid Mech.* **225**, 1.